

Alteration of lipid bilayer mechanics by volatile anesthetics: insights from s-long molecular dynamics simulations

*Original*

Alteration of lipid bilayer mechanics by volatile anesthetics: insights from s-long molecular dynamics simulations / Zizzi, E.A., Cavaglia', M., Tuszynski, J.A., Deriu, M.A.. - In: ISCIENCE. - ISSN 2589-0042. - ELETTRONICO. - (2022). [10.1016/j.isci.2022.103946]

*Availability:*

This version is available at: 11583/2955776 since: 2022-02-18T19:04:12Z

*Publisher:*

Cell Press

*Published*

DOI:10.1016/j.isci.2022.103946

*Terms of use:*

This article is made available under terms and conditions as specified in the corresponding bibliographic description in the repository

*Publisher copyright*

Elsevier postprint/Author's Accepted Manuscript

© 2022. This manuscript version is made available under the CC-BY-NC-ND 4.0 license  
<http://creativecommons.org/licenses/by-nc-nd/4.0/>. The final authenticated version is available online at:  
<http://dx.doi.org/10.1016/j.isci.2022.103946>

(Article begins on next page)

# Journal Pre-proof



Alteration of lipid bilayer mechanics by volatile anesthetics: insights from  $\mu$ s-long molecular dynamics simulations

Eric A. Zizzi, Marco Cavaglià, Jack A. Tuszynski, Marco A. Deriu

PII: S2589-0042(22)00216-4

DOI: <https://doi.org/10.1016/j.isci.2022.103946>

Reference: ISCI 103946

To appear in: *ISCIENCE*

Received Date: 2 August 2021

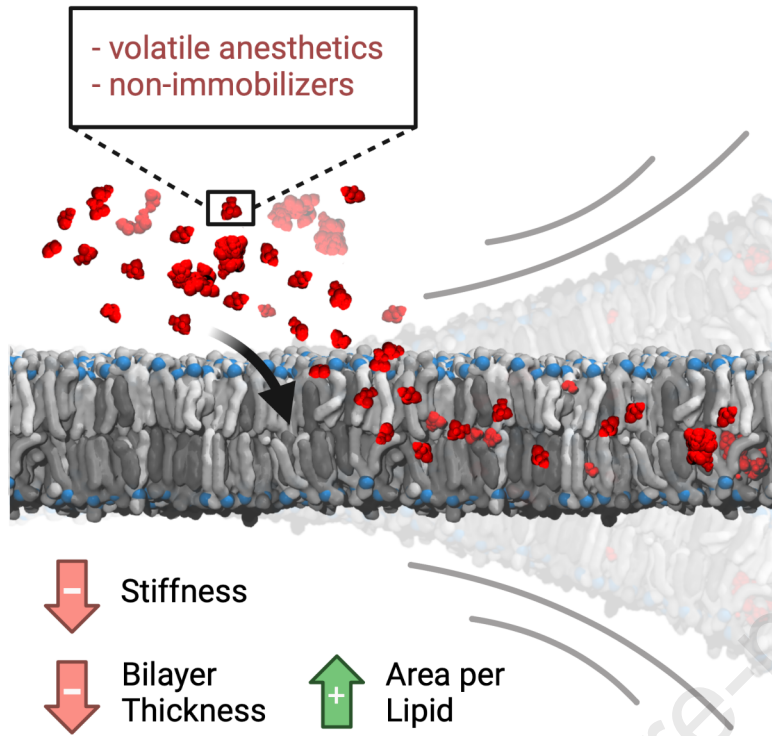
Revised Date: 25 January 2022

Accepted Date: 15 February 2022

Please cite this article as: Zizzi, E.A., Cavaglià, M., Tuszynski, J.A., Deriu, M.A., Alteration of lipid bilayer mechanics by volatile anesthetics: insights from  $\mu$ s-long molecular dynamics simulations, *ISCIENCE* (2022), doi: <https://doi.org/10.1016/j.isci.2022.103946>.

This is a PDF file of an article that has undergone enhancements after acceptance, such as the addition of a cover page and metadata, and formatting for readability, but it is not yet the definitive version of record. This version will undergo additional copyediting, typesetting and review before it is published in its final form, but we are providing this version to give early visibility of the article. Please note that, during the production process, errors may be discovered which could affect the content, and all legal disclaimers that apply to the journal pertain.

© 2022 The Author(s).



# Alteration of lipid bilayer mechanics by volatile anesthetics: insights from $\mu$ -long molecular dynamics simulations

Eric A. Zizzi<sup>1</sup>, Marco Cavaglià<sup>1</sup>, Jack A. Tuszynski<sup>1,2</sup>, Marco A. Deriu<sup>1,\*</sup>

<sup>1</sup> *Polito<sup>BIO</sup>Med Lab, Department of Mechanical and Aerospace Engineering, Politecnico di Torino, 10129 Turin, Italy*

<sup>2</sup> *Department of Physics, University of Alberta, Edmonton, AB, Canada*

\*Correspondence: [marco.deri@polito.it](mailto:marco.deri@polito.it)

**Lead Contact:** Marco A. Deriu, [marco.deri@polito.it](mailto:marco.deri@polito.it)

## Summary

Very few drugs in clinical practice feature the chemical diversity, narrow therapeutic window, unique route of administration and reversible cognitive effects of volatile anesthetics. The correlation between their hydrophobicity and their potency and the increasing amount of evidence suggesting that anesthetics exert their action on transmembrane proteins, justifies the investigation of their effects on phospholipid bilayers at the molecular level, given the strong functional and structural link between transmembrane proteins and the surrounding lipid matrix. Molecular dynamics simulations of a model lipid bilayer in the presence of ethylene, desflurane, methoxyflurane and the non-immobilizer 1,2-dichlorohexafluorocyclobutane (also called F6 or 2N) at different concentrations highlight the structural consequences of VA partitioning in the lipid phase, with a decrease of lipid order and bilayer thickness, an increase in overall lipid lateral mobility and area-per-lipid, and a marked reduction in the mechanical stiffness of the membrane, that strongly correlates with the compounds' hydrophobicity.

## Introduction

Volatile anesthetics (VAs) are a diverse set of compounds routinely used in medical practice to induce and/or sustain a reversible state of suspended consciousness, analgesia and amnesia. Despite the fact that modern surgery would hardly be imaginable without such compounds, little is known about their mechanism of action, especially at the molecular level. This is partly due to the high chemical and physical diversity of available VAs, which range from single-atom gases such as Xenon, to more complex molecules such as halogen-substituted ethers and even steroids. In the past decades, several different theories of anesthetic action have been proposed with the aim of explaining anesthetic behavior despite this lack of structural similarity, starting from the Meyer-Overton correlation between the lipid solubility of VAs and their clinical potency (in terms of Minimum Alveolar Concentration, MAC). This theory paved the way towards what is known as the lipid theory, which postulates that the main mechanism of action of anesthetics lies in the alteration of the structure

35 of lipid bilayers – in particular cell membranes – in a non-specific fashion (Meyer, 1937). Some shortcomings  
36 of this hypothesis, including the lack of any anesthetic effect of other lipid-altering factors, e.g. temperature,  
37 steered the interest of research around anesthesia towards finding specific molecular targets – i.e. proteins –  
38 which could explain the clinical effects of VAs. Indeed, an increasing amount of evidence points toward ion  
39 channels located in the Central Nervous System as relevant targets for anesthetics, starting from the works of  
40 Franks and Lieb (Franks and Lieb, 1994, 1984). A detailed review of molecular targets of anesthetics can be  
41 found in Campagna et al. (Campagna et al., 2003). Interestingly, despite the increasing evidence of interactions  
42 with ion channels, the exact mechanism of action remains unclear, and researchers failed to agree on the most-  
43 relevant effectors of anesthesia at clinically relevant VA concentrations. In most works, the two  
44 aforementioned approaches to explaining anesthesia – the lipid theory and the receptor theory – are largely  
45 regarded as irreconcilable. What seems often overlooked however, is the intimate connection between  
46 transmembrane receptors such as ion channels and their surrounding lipid environment, which highlights the  
47 duality, rather than the contrast, of the two theories. Indeed, the membrane-spanning portions of integral  
48 membrane proteins are known to be affected by the surrounding lipids, so that the conformational  
49 characteristics of specific sections of the transmembrane regions may change in response to alterations of the  
50 lipid bilayer. It has been shown for example that bilayer thickness can directly influence protein activity (De  
51 Planque and Killian, 2003; Mouritsen and Bloom, 1993). Conversely, there is increasing experimental  
52 evidence that the presence of proteins embedded in the membrane has profound effects on the latter's  
53 stabilization, mediated mainly by hydrophobic interactions (Dumas et al., 1999). At higher scales, the  
54 reciprocal interaction of the membrane's lipid environment and embedded proteins has also been shown to be  
55 mediated by so-called lipid rafts (Lingwood and Simons, 2010), which are sub- $\mu\text{m}$  domains of spatially  
56 organized lipids, typically sphingomyelin and cholesterol (Allen et al., 2006; Levental et al., 2011; Moon et  
57 al., 2017).

58 It appears thus entirely reasonable that an interaction of increasingly hydrophobic compounds, such as VAs,  
59 within biological membranes might have significant effects on membrane organization and structure, but at  
60 the same time this cannot happen without altering the energetic landscape of the interactions between  
61 membranes and transmembrane receptors. The idea that small solutes such as VAs bear the potential of altering  
62 the mechanics and thermodynamics of the lipid bilayer, with possible consequences on the dynamics of  
63 embedded proteins, was already introduced in the work of Cantor (Cantor, 1999), who elegantly discussed the  
64 possible relevance of lateral pressure profiles within the lipid bilayer and suggested the mechanistic link  
65 between anesthetics, the lipid bilayer and embedded ion channels (Cantor, 1997). Indeed, earlier molecular  
66 dynamics simulations by Huang et al. had predicted a possible structural effect of anesthetics within the  
67 phospholipid bilayer, in the form of an increased lateral diffusion of lipids and an increase in the overall fluidity  
68 of the bilayer (Huang and Bertaccini, 1995). More recently, following earlier speculations suggesting a role of  
69 lipid rafts in anesthesia (Gray et al., 2013; Lee, 1976; Lerner, 1997), Pavel et al. demonstrated a membrane-  
70 mediated effect of anesthetics, whereby the anesthetic-induced alteration of lipid raft organization is able to  
71 modulate the sensitivity of channel proteins to anesthetics (Pavel et al., 2020). In addition to these

72 considerations, the direct effect of anesthetics on transmembrane receptors might be exerted within the  
73 transmembrane portion of the receptors rather than on the intracellular or extracellular domains alone and  
74 might thus be connected to the ability of compounds to partition inside the membrane and laterally diffuse  
75 within the lipid phase prior to interacting directly with cryptic, hydrophobic sites on the target. As a matter of  
76 fact, compounds that are more soluble in oil-like media, as is the case for VAs as shown by the Meyer-Overton  
77 correlation, tend to partition inside the membrane rather than in aqueous solutions, and vice versa.

78 In the context of investigating the properties of lipid bilayers, a vast literature exists exploring the behavior of  
79 model phospholipid membranes in different physical contexts and the structural and functional link between  
80 membranes and embedded proteins and peptides. Indeed, it is well-known that the structure of phospholipid  
81 bilayers has strong functional consequences (Zhuang et al., 2014). The structural parameters usually reported  
82 in both experimental and computational studies include (a) the Area-per-Lipid (APL), which can be calculated  
83 from molecular densities or geometrically from the membrane patch surface; (b) the bilayer thickness  $\delta$ , which  
84 is directly related to the APL; (c) deuterium order parameters ( $S_{CD}$ ), which provide quantitative evidence of  
85 lipid chain order and the membrane rigidity resulting from this; (d) direct measures of the mechanical  
86 characteristics of the membrane, such as the bilayer bending modulus ( $K_c$ ). Due to the limitations, both  
87 methodological and economical, of experimental settings aimed at investigating such properties for a vast array  
88 of model membranes in different physical and biochemical contexts, computational approaches such as  
89 molecular dynamics (MD) have proven a valuable tool for exploring and rationalizing the structural  
90 characteristics and interaction phenomena within model bilayers at the molecular level. While a great number  
91 of computational investigations employed single-component lipid patches (Grasso et al., 2018; Huang and  
92 Bertaccini, 1995; Tang and Xu, 2002), mostly of phosphatidylcholines (PCs) or phosphatidylethanolamines  
93 (PEs), recent advances in lipid force fields (Dickson et al., 2014, 2012; Jämbeck and Lyubartsev, 2012; Klauda  
94 et al., 2010; Pluhackova et al., 2016) and the increasing power of computational resources have paved the way  
95 for the simulation of complex, composite bilayers formed by multiple lipid species and varying cholesterol  
96 concentrations, both at all-atom (AA) and coarse-grained (CG) resolutions (Ingólfsson et al., 2017 and  
97 references therein).

98 With this in mind, the present work focuses on investigating the interaction between volatile anesthetics and a  
99 composite model mammalian cell membrane through the use of computational molecular modelling, to explore  
100 the effects of VAs on lipid bilayers. With the goal of exploring the effect of a chemically and physically diverse  
101 set of hydrophobic compounds spanning a wide range of clinical potencies, we carried out simulations with  
102 desflurane (2-(difluoromethoxy)-1,1,1,2-tetrafluoroethane), a fluorinated ether with a MAC of 6% (Riazi and  
103 Ibarra Moreno, 2013), methoxyflurane (2,2-dichloro-1,1-difluoro-1-methoxyethane), a potent halogenated  
104 methyl ethyl ether with a MAC value of 0.16%, now largely abandoned in the light of its nephrotoxicity  
105 (Mazze, 1971), and ethylene, which is only mildly anesthetic with a MAC value of 67% (Miller et al., 1969).  
106 Simulations were also carried out with F6 (1,2-dichlorohexafluorocyclobutane), a widely investigated  
107 nonimmobilizer which does not follow the Meyer-Overton correlation in that it does not induce complete

108 anesthesia as would be expected from its lipophilicity, but it has been demonstrated to induce amnesia (Eger  
109 et al., 2001; Perouansky et al., 2007; Taylor et al., 1999).

110 A graphical summary of the model membrane and of the simulated VAs is reported in Figure 1.

## 111 **Results**

### 112 **Potent VAs alter the membrane structure upon partitioning**

113 To quantitatively assess both the quality of the membrane model itself and the effect of volatile anesthetics on  
114 overall membrane structure, the geometric Area per Lipid (gAPL) and Bilayer Thickness ( $\delta$ ) were evaluated  
115 and are reported for all systems in detail in Table 1. The former is a crucial parameter influencing lipid diffusion  
116 profiles, lipid chain order and overall membrane elastic properties. It also represents a metric to assess the  
117 reached equilibrium of membrane simulations, along with the closely related bilayer thickness. The control  
118 simulation without any ligands yielded an average gAPL of  $42.89 \text{ \AA}^2$  (95% CI:  $42.83 - 42.95 \text{ \AA}^2$ ) and an  
119 average bilayer thickness of  $46.85 \text{ \AA}$  (95% CI:  $46.81 - 46.89 \text{ \AA}$ ), and proved consistent both with previous  
120 computational studies of membranes with similar lipid composition and comparable cholesterol content (Klähn  
121 and Zacharias, 2013; Saeedimazine et al., 2019; Shahane et al., 2019b) and with experimental data on  
122 cholesterol-enriched membranes (Maulik and Shipley, 1996), although it is to be noted that bilayer thickness  
123 heavily depends on the specific bilayer composition (Li et al., 2012) and experimental data of membranes with  
124 the exact lipid composition of the present model is, to the best of our knowledge, not available. Nevertheless,  
125 the reduced gAPL and  $\delta$  values are consistent with the high cholesterol content ( $\sim 34\%$ ) inducing membrane  
126 condensation, as demonstrated in earlier literature (Hofsäß et al., 2003; Leftin et al., 2014; Meyer and Smit,  
127 2009; TJ, 1978).

128 Figure 2 shows the effect of increasing ligand concentrations on both gAPL and thickness. In the case of  
129 ethylene (Figure 2A) no significant effect of ligand concentration on bilayer thickness is observed (from  $46.85$   
130  $\text{ \AA}$  to  $46.52 \text{ \AA}$ ), with only a mild increase in area per lipid, which reaches  $45.16 \text{ \AA}^2$  with 50% ethylene.  
131 Desflurane (Figure 2B) and methoxyflurane (Figure 2C) on the other hand induce a marked reduction in bilayer  
132 thickness down to  $45.67 \text{ \AA}$  with 50% desflurane and  $45.16 \text{ \AA}$  with 50% methoxyflurane, despite the steric  
133 hindrance of the high number of ligand molecules partitioned within the membrane. At the same time, these  
134 two anesthetics induce a marked increase in gAPL, up to  $48.18 \text{ \AA}^2$  and  $48.53 \text{ \AA}^2$  for systems with 50%  
135 desflurane and methoxyflurane, respectively. Overall, the latter two ligands induce a progressive reduction of  
136 membrane thickness, along with a lateral spreading of the lipids on the xy plane, both in a fashion proportional  
137 to ligand concentration. This effect is totally absent for ethylene concentrations up to 25%, with only a mild  
138 increase in gAPL induced at 50% and no measurable thickness reduction effect. These results are in agreement  
139 with earlier computational studies reporting a significant lateral expansion and simultaneous thickness  
140 contraction induced in lipid membranes by halothane, another VA, over a wide range of molar fractions (Koubi  
141 et al., 2000; Pickholz et al., 2005; Tu et al., 1998). Lastly, simulations with the nonimmobilizer F6 (Figure 2D)  
142 highlight a reduction in bilayer thickness (from  $46.85 \text{ \AA}$  to  $45.52 \text{ \AA}$  with 50% F6) comparable to the simulations

143 with desflurane and methoxyflurane, whereas the increase in gAPL is more subdued at higher concentrations,  
144 reaching at most  $46.44 \text{ \AA}^2$  with 50% F6.

145 The increase in gAPL induced by ligand partitioning came alongside an increase in spontaneous water  
146 permeation through the membrane, reported as the number of water molecules crossing the bilayer per  
147 microsecond in Table 1: throughout the control simulation a water permeation frequency of 16 water  
148 molecules/ $\mu\text{s}$  was observed, whereas this frequency increased to up to 285 molecules/ $\mu\text{s}$  and 391 molecules/ $\mu\text{s}$   
149 in the case of 50% desflurane and 50% methoxyflurane, respectively. Conversely, just as for gAPL and bilayer  
150 thickness, more subdued differences were observed with ethylene, with at most 112 molecules/ $\mu\text{s}$  at the highest  
151 concentration of 50%. Throughout the simulations with F6, a permeation frequency of up to 206 molecules/ $\mu\text{s}$   
152 was observed at 25% simulated fraction, with a slightly lower frequency of 155 molecules/ $\mu\text{s}$  at 50%  
153 concentration, consistent with the trends of gAPL and bilayer thickness. Despite the increase in spontaneous  
154 permeation frequency with increasing ligand concentrations, no pore formation was observed throughout the  
155 whole set of simulations, with no disruption of the overall structural integrity of the bilayer.

#### 156 **Anesthetics and nonimmobilizers are predicted to have specific localization areas within the bilayer**

157 The partitioning of ligands inside the lipid bilayer not only plays a crucial role in ligand-receptor interaction  
158 with transmembrane proteins (Vauquelin and Packeu, 2009), but can also significantly alter the bilayer's  
159 structural and mechanical properties (Koubi et al., 2000; Tsuchiya and Mizogami, 2013; Tu et al., 1998;  
160 Yamamoto et al., 2012). The analysis of the density distributions of the different membrane components and  
161 of the ligands along the z coordinate highlights a marked tendency of the four ligands to partition inside the  
162 bilayer in specific hydrophobic regions.

163 **Error! Reference source not found.** reports the density distributions for the control simulation (Figure 3A)  
164 and the simulations at the highest concentration of ethylene (Figure 3B), desflurane (Figure 3C),  
165 methoxyflurane (Figure 3D) and F6 (Figure 3E). The corresponding plots for 12.5% and 25% ligand  
166 concentrations, which highlight the same qualitative distribution pattern, are reported in Supplementary Figure  
167 S1 and S2, respectively. For desflurane and methoxyflurane, three main areas of localization clearly emerge:  
168 the main peak is located at the bilayer center, corresponding to the minimum of lipid tail density. This is  
169 consistent with the hydrophobic nature of these compounds, and explains why the massive ligand partitioning  
170 inside the membrane does not result in a simultaneous increase in bilayer thickness, as would be expected by  
171 the effect of steric hindrance and molecular volume alone. Indeed, due to the low lipid tail density in the  
172 membrane core, resulting in less occupied molecular volume, many freely diffusing hydrophobic species are  
173 known to temporarily localize in this region, including cholesterol during flip-flop transitions (Bennett et al.,  
174 2009). The secondary peaks on the other hand are located near the membrane-water interface, immediately  
175 below the glycerol groups. This is in agreement with earlier computational findings by Pohorille et al., who  
176 predicted this very area of localization to be involved in the molecular mechanism of anesthesia  
177 (Christophe Chipot et al., 1997; Pohorille et al., 1998, 1996). Interactions of volatile anesthetics near the  
178 water-lipid interface region have also been reported in the past by Tang and Xu, who employed MD

179 simulations to evaluate the effect of halothane on a gramicidin A channel protein embedded in a DMPC bilayer  
180 (Tang and Xu, 2002). While these earlier simulations employed more simplistic membrane models composed  
181 of a single lipid type, and investigated remarkably lower timescales, the localization near the water/lipid  
182 interface is herein predicted to partially occur also in our composite, cholesterol-enriched membrane model,  
183 albeit not as predominantly as the localization at the membrane core. On the contrary, in the case of F6, the  
184 localization at the interface appeared comparable to that at the membrane core, resulting in a different density  
185 pattern with respect to the other compounds, with no predominant peak at the membrane core. These findings  
186 are consistent with the different effects observed for F6 on gAPL with respect to the VAs.

187 Quantitative measures of the tendency of ligands to reside inside the lipid bilayer with respect to the aqueous  
188 solvent are reported in literature in the form of either ligand equilibrium partition coefficients (Vauquelin and  
189 Packeu, 2009) – usually calculated as the ratio between the ligand concentration in the solvent and the  
190 concentration within the membrane – or directly as molar (Herold et al., 2017) or molal (Seeman, 1972) ligand  
191 concentration inside the membrane. Whatever the metric, these quantities depend, among others, on the  
192 chemical and physical nature of the ligand itself, in particular its hydrophobicity and the presence of  
193 hydrophilic moieties, on the temperature of the membrane, i.e. its phase state, and on the membrane cholesterol  
194 concentration (Vauquelin and Packeu, 2009).

195 To provide a direct quantitative measurement of the amount of ligand able to dissolve into the membrane,  
196 Figure 4 reports the molal concentration reached by the four simulated ligands within the lipid bilayer. Results  
197 confirm that the concentration of ligands inside the membrane increases with increasing amounts of simulated  
198 ligand molecules, as expected by the physical characteristics of these compounds. One notable exception is  
199 represented by F6 (dotted bars in Figure 4), whose concentration inside the bilayer is comparable to that of the  
200 other compounds at 12.5% and 25% simulations, reaching up to 0.35 mol/kg (at 25% simulated molar fraction,  
201 95% CI 0.33 – 0.37), but showing no further increase in the case of 50% simulations, plateauing at 0.30 mol/kg  
202 (95% CI 0.20 – 0.40) and with a considerable amount of ligand aggregating in the water phase without entering  
203 the membrane. Also, the analysis of ligand concentration inside the membrane highlights that ethylene (white  
204 bars in Figure 4) also partitioned inside the bilayer, albeit at lower rates in the 12.5% and 25% simulations.  
205 Conversely, when simulated at 50% molar fraction, the reached concentration (0.535 mol/kg, 95% CI: 0.529-  
206 0.541) is comparable to the one of desflurane (patterned bars in Figure 4, 0.621 mol/kg, 95% CI: 0.385-0.856)  
207 and methoxyflurane (shaded bars in Figure 4, 0.596 mol/kg, 95% CI: 0.355-0.837). Also, it is worth noting  
208 how the considerable number of ligands present at 50% molar fraction leads to greater fluctuations in ligand  
209 partitioning in the case of the latter two ligands, but not in the case of ethylene. This is a consequence of the  
210 key differences in behavior between ethylene and the other simulated ligands: firstly, ethylene does not form  
211 aggregates in the water phase even at 50% concentration as opposed to the other three ligands. Indeed,  
212 desflurane and methoxyflurane are observed to enter the membrane in the form of aggregates of up to tens of  
213 molecules, while F6 forms aggregates at 50% concentration that are partially unable to enter the bilayer and  
214 remain in the water phase throughout the simulations, resulting in lower overall membrane partitioning (see  
215 dotted bars in Figure 4). Secondly, ethylene did not show the secondary localization areas below the glycerol

216 groups inside the membrane (see Figure 3), which are instead present for the other three ligands, but rather  
217 preferably positions itself at the membrane core, making ligand exchange between the membrane and the water  
218 phase less frequent.

### 219 **VAs and F6 decrease lipid chain order already at 12.5% molar fraction**

220 Deuterium order parameters  $S_{CD}$  represent a quantitative measurement of lipid packing and provide insights  
221 into the mobility of the hydrophobic chains. Data for POPC from the control simulation without ligands (Figure  
222 5, blue lines) is in good agreement with recently published results of compositionally similar, cholesterol- and  
223 sphingomyelin-enriched POPC/POPE membranes (Saeedimazine et al., 2019), and confirms the membrane-  
224 ordering effect induced by cholesterol. Conversely, in the presence of desflurane (Figure 5B and F) and  
225 methoxyflurane (Figure 5C and G), the mechanical consequence of ligand partitioning within the hydrophobic  
226 core as well as below the glycerol groups is a reduction in acyl chain order parameters, with a trend proportional  
227 to the ligand concentration (Figure 5). This behavior is also present in the simulations with F6, (Figure 5D and  
228 h), with the exception of simulations at 50% molar fraction, where the effect of the ligand on lipid chain order  
229 is comparable within error to that at 25% concentration. This is coherent with the finding that there are no  
230 remarkable differences in the concentration reached by F6 within the bilayer at 25% and 50% simulated molar  
231 fraction (see results above), hence a comparable effect on lipid packing is not unexpected.

232 The effect on lipid order is more subdued in the case of ethylene (Figure 5A and D), where the decrease in  $S_{CD}$   
233 is particularly evident only at 50% concentration, with only marginal reductions ( $< 0.01$ ) at lower ligand  
234 concentrations. These trends, reported in Figure 5 for POPC, are analogous for the other lipid species included  
235 in the employed membrane model (see Supplementary Information), and hint at a membrane-destabilizing  
236 effect of ligand partitioning, with consequences on overall bilayer mechanics.

### 237 **Desflurane, methoxyflurane and F6 decrease membrane bending rigidity in a concentration-dependent** 238 **manner**

239 In the light of the ligands' tendency to partition inside the lipid bilayer, and of the structural consequences  
240 thereof observed by the analysis of area per lipid, bilayer thickness and acyl chain order parameters, a more  
241 specific quantification of the bilayer's mechanical characteristics was carried out by directly determining the  
242 bilayer bending modulus using a previously proposed methodology relying on the analysis of lipid splay.

243 The bilayer bending modulus for the control simulation is 88.80 kT (95% CI: 87.16 – 90.44), and while a direct  
244 comparison with other computational and experimental studies is often not trivial due to the differences in  
245 membrane composition, temperature and methodology, this result is remarkably consistent with earlier studies  
246 of membranes with similar cholesterol content (around 0.3 molar fraction) which induces structural  
247 condensation of the lipid phase yielding a considerable increase in membrane stiffness and a shift towards the  
248 liquid-ordered phase (Khelashvili et al., 2013; Subczynski et al., 2017). Furthermore, the obtained value for  
249 the control simulation agrees with earlier literature reporting experimentally determined stiffness values for

250 plasma membrane vesicles (PMVs,  $K_c = 99.75$  kT), which are representative systems of the pure plasma  
251 membrane *in vitro* (see (Pontes et al., 2013) and references therein).

252 The trend of reduction of bilayer bending stiffness at increasing anesthetic concentrations is visible in Figure  
253 6A. At 12.5% anesthetic concentration, the presence of desflurane, methoxyflurane and F6 leads to a reduction  
254 in monolayer bending stiffness by 12.01%, 19.44% and 11.78%, respectively, compared to a mere 2.10%  
255 reduction with ethylene. At 25% anesthetic concentration, the bending stiffness is reduced by 20.80% and  
256 26.95% by desflurane and methoxyflurane, respectively, and by 20.20 % with F6, compared to a limited 2.48%  
257 reduction caused by ethylene. Lastly, in the simulations with 50% anesthetic molar fraction, the bending  
258 stiffness is reduced by 28.38% with desflurane and 28.30% by methoxyflurane, while the effect of F6 remains  
259 again comparable to the 25% simulation, yielding a reduction of the bilayer bending modulus of 19.98%. Only  
260 at this higher concentration does ethylene lead to a noticeable reduction in bending stiffness by 15.32%. This  
261 is consistent with order parameter results, which showed a decrease in lipid tail packing in the presence of  
262 ethylene only at 50% concentration (see Figure 5).

263 Overall, the trends in reduction in membrane bending stiffness are consistent with the hydrophobicity of these  
264 compounds. From the analysis of the data from the 12.5% concentration simulations, which is the closest to  
265 clinical concentrations, a linear relationship emerges between the lipophilicity of the ligands – quantified by  
266 the octanol/water partition coefficient  $\log(K_{o/w})$  – and the reduction in bilayer stiffness ( $\Delta K_c$ ) observed in  
267 simulations ( $R^2 = 0.95$ , Figure 6B). Interestingly this relationship seems to hold true also for F6, which is not  
268 an anesthetic but a convulsant with amnesic properties, supporting the hypothesis that the alteration of bilayer  
269 mechanics might not be *per se* the mechanistic cause of anesthesia, but might be implicated in some of the  
270 effects caused by these compounds, especially at *supra*-clinical concentrations.

## 271 Discussion

272 In the present work, we employed long all-atom molecular dynamics simulations to assess the structural effects  
273 of the volatile anesthetics desflurane, methoxyflurane, ethylene, a low-potency control, and the  
274 nonimmobilizer F6 on a model composite lipid bilayer composed of POPC, POPE, POPS, PSM and  
275 cholesterol. Anesthetics rapidly partition inside the bilayer, reaching intra-membrane concentrations of  
276 approximately 0.6 molal, while F6 is unable to reach concentrations higher than 0.3 molal even when simulated  
277 at 50% ligand/lipid molar fraction. Desflurane and methoxyflurane preferentially localize at the membrane  
278 core region and immediately below the glycerol groups of the bilayer, with structural consequences on both  
279 area per lipid and bilayer thickness. Indeed, the partitioning of ligands causes a contraction in bilayer thickness  
280 while at the same time reducing lateral condensation and causing an increase in area per lipid and in  
281 spontaneous water permeation, albeit with no pore formation or disruption of overall membrane integrity. The  
282 convulsant F6 shows a different localization pattern within the membrane, with preferential interaction below  
283 the lipid/water interface and a less prominent residency at the membrane core region, but with similar structural  
284 effects with respect to the aforementioned VAs. The structural rearrangement of the membrane has direct  
285 consequences on its mechanical properties, as testified by a progressive reduction in lipid hydrocarbon chain

286 packing. The reduced energetic cost of splaying adjacent lipid tails caused by ligand partitioning leads to a  
287 reduction in bilayer bending rigidity in a fashion proportional to ligand concentration. These structural effects  
288 are not observed for ethylene at a molar ratio of up to 0.25 with respect to the lipids, with only marginal effects  
289 at 0.5 molar ratio. Consistently with these considerations, ethylene also constitutes the least hydrophobic  
290 among the three studied VAs. It is to be underlined how the non-immobilizer F6 caused a comparable reduction  
291 in bilayer bending rigidity despite its lack of potency as a general anesthetic. Hence, also bearing in mind that  
292 the simulated concentrations are above the typical concentrations reached in clinical settings, these findings  
293 shed light on important aspects of anesthetic-membrane interactions. Firstly, the two potent VAs and the  
294 nonimmobilizer F6 studied herein have, even at the smallest studied concentration, the capacity to alter the  
295 energetic landscape of a model mammalian lipid bilayer, which results in profound changes of its mechanical  
296 characteristics in terms of a marked reduction in bending stiffness and an overall shift towards a liquid-  
297 disordered phase, as shown by the reduction in thickness, the increase in APL, the increase in spontaneous  
298 water permeation and the reduction of lipid chain order. This effect appears as antagonistic to the role of  
299 cholesterol, which induces instead a shift towards the liquid-ordered phase and an overall increase in  
300 membrane rigidity (Subczynski et al., 2017). Interestingly, VAs and cholesterol seem to have instead a similar  
301 effect in the context of lipid raft microdomains, whose number and size has been recently shown to increase  
302 with both anesthetics and cholesterol (Pavel et al., 2020). Given the fundamental role of the cell membrane  
303 not only in overall cell mechanics and structural stability, but also in the function of several transmembrane  
304 proteins, including important ion channels thought to be directly involved in anesthesia or its side effects  
305 (Bertaccini, 2010; Bertaccini et al., 2013; Franks and Lieb, 1994; Herold and Hemmings, 2012; Yamakura et  
306 al., 2003), it appears entirely reasonable that bilayer alterations might be, directly or indirectly, involved in  
307 some of the effects exerted by VAs and F6, in the same way in which cholesterol is a crucial modulator of  
308 membrane mechanics and essential for many membrane functions. As a matter of fact, a hybrid protein/lipid  
309 mechanism based on the alteration of the physics of the lipid membrane has been recently proposed by Pavel  
310 et al., who described and demonstrated *in vivo* the indirect effect of volatile anesthetics on membrane-  
311 embedded channel proteins by means of an alteration of sphingomyelin lipid rafts (Pavel et al., 2020). Despite  
312 failing to highlight any effect of VAs on pure DOPC liposomes, employed as a model system of the pure  
313 membrane, the research provided further evidence for the key role of membrane biophysics in the molecular  
314 mechanisms of anesthetics, and supports the speculation that anesthetics directly interact with the phospholipid  
315 membrane, with diversified effects not only at different time and length scales, e.g. on local lipid arrangement  
316 vs. on larger-scale lipid microdomains, but also at different concentrations, e.g. clinical vs. *supra*-clinical.  
317 Indeed, not only does the alteration of the surrounding lipid environment bear the potential of altering the  
318 function of channel proteins, e.g. by modifying the energetic cost of key functional motions, but the rapid  
319 partitioning of VAs into the hydrophobic core might also be an essential prerequisite for anesthetics to reach  
320 cryptic hydrophobic binding sites of such proteins within regions embedded in the membrane, which are  
321 inaccessible from the external water phase. In this sense, the findings reported herein do not clash with earlier  
322 evidence of a direct action of anesthetics on ion channels (John Mihic et al., 1997; Mascia et al., 2000), which

323 is still debated to be the final mechanism of action causative of anesthesia. Instead, the computational  
324 predictions provide a quantification of the interaction between VAs and the lipid phase and the mechanical  
325 alterations of the latter at increasing VA concentrations. This mechanism might thus be necessary, but arguably  
326 not sufficient, for a compound to exhibit anesthetic potency, thereby explaining both the Meyer-Overton  
327 correlation and outliers thereof such as nonimmobilizers, featuring considerable hydrophobicity but low to no  
328 anesthetic potency. This is confirmed by analyzing the effect on bilayer mechanics of the nonimmobilizer F6,  
329 which is herein predicted to alter membrane behavior in a similar manner to potent anesthetics. This further  
330 suggests that the alteration of the lipid membrane *per se* is unlikely to be the sole mechanistic cause of  
331 anesthesia as a whole. Rather, it might be a biophysical mechanism involved in some of the effects that are  
332 exerted both by anesthetic agents and nonimmobilizers such as F6, which has been shown e.g. to induce  
333 convulsions and amnesia *in vivo*. Also, the direct action on membrane mechanics might rather provide a  
334 mechanistic basis to explain the side effects of anesthetics, which arise at higher concentrations and are in  
335 common with convulsants (Koblin et al., 1981; Modica et al., 1990). Indeed, given the exacerbation of the  
336 alteration of bilayer structure and mechanics predicted herein at such higher concentrations – 0.25 and 0.5  
337 molar fractions –, it is reasonable that such a mechanism might be involved in the molecular basis of the side  
338 effects of VAs at *supra*-clinical concentrations.

### 339 **Conclusions**

340 The molecular mechanisms of general anesthesia are to this day an unsolved medical puzzle. While recent  
341 literature generally considers transmembrane proteins as the main functional target of volatile anesthetics, the  
342 Meyer-Overton correlation clearly hints at the ability of these compounds to interact with the lipid bilayer of  
343 cell membranes, even if the final functional action is not exerted directly on the membrane itself. Long  
344 molecular dynamics simulations of the three VAs ethylene, desflurane and methoxyflurane and of the  
345 nonimmobilizer F6 confirm the strong tendency of these ligands to partition within the hydrophobic  
346 environment of a model membrane, and allowed to quantify the structural effects this determines: a reduction  
347 in bilayer thickness, a decrease in lipid chain order and a reduction of membrane stiffness, with a trend  
348 proportional to the amount of partitioned ligands. Given the strong correlation observed between the  
349 compounds' lipophilicity and the reduction in the membrane bending modulus caused by their inclusion within  
350 the membrane, it appears that the phospholipid membrane might be a key component in determining some of  
351 the effects of anesthetics on channel proteins, by altering their structural and mechanical characteristics in the  
352 presence of VAs with possible consequences on embedded protein function and on the intracellular link  
353 between the membrane and the cytoskeleton. Moreover, the remarkable tendency to dissolve in the lipid phase  
354 followed by lateral diffusion within the membrane, might be an essential step to reach key functional  
355 hydrophobic binding pockets in transmembrane proteins, which would be inaccessible from the aqueous  
356 solvent, such as some transmembrane domains which have been shown to bind anesthetics (Mascia et al.,  
357 2000). These considerations are well in line not only with the strong relationship between potency and  
358 hydrophobicity, but also with the most recent theories indicating ion channels as ultimate targets for general  
359 anesthetics, and pointing at the lipid environment of the membrane as a first transducer of anesthetic action

360 (Pavel et al., 2020). At the same time, the functional distinction between general anesthetics and compounds  
361 without any anesthetic effect but high lipophilicity, such as F6, might involve processes and molecular players  
362 downstream of the interaction with the membrane. This concept highlights how the lipid-centered and the  
363 protein-centered theories of anesthetic action are not, in fact, irreconcilable, but might rather be two aspects of  
364 a composite mechanism, which sees the interaction with the lipid membrane as a necessary but perhaps not  
365 sufficient condition. A more thorough analysis of how this occurs and to which extent, especially as to where  
366 the discrimination between general anesthetics and non-anesthetic Meyer-Overton outliers takes place, as well  
367 as of the effect of the membrane alteration on the cytoskeleton linked at the intracellular interface, certainly  
368 warrants further computational and experimental investigations, and seems well worth pursuing further.

### 369 **Limitations of the Study**

- 370 • While the membrane model employed in this work is a multi-component membrane which accounts  
371 for the major lipid constituents of mammalian cell membranes, it still represents a simplified  
372 representation, especially in the context of neural membranes which include several types of different  
373 phosphatidylcholines, phosphatidylethanolamines, sphingomyelins, phosphatidylserines, glycolipids,  
374 cerebroside and phosphatidylinositols, just to name a few. Building increasingly realistic models of  
375 cellular membranes is an active topic of research and requires major computational efforts, often  
376 demanding the use of coarse-grained modelling and extended parameter validations to accurately  
377 capture the physical and chemical characteristics of the simulated species.
- 378 • The present work focuses on the effects of three different VAs of different chemical structure and  
379 spanning a wide range of clinical potencies. However, several other VAs exist that were not included  
380 in the present work, and are very well worth investigating in further studies. Also, we herein included  
381 a compound that would be expected to have high potency as an anesthetic based on its hydrophobicity  
382 and structural similarity to actual VAs, but actually lacks any anesthetic effect, namely F6. Given the  
383 comparable effect of this compound on pure membrane mechanics, further investigations are needed  
384 to explore downstream events (e.g. the interaction with transmembrane proteins) that would ultimately  
385 set apart potent anesthetics from hydrophobic nonimmobilizers and other similar negative controls.

### 386 **Acknowledgments**

387 We acknowledge the CINECA award under the ISCRA initiative, for the availability of high-performance  
388 computing resources and support.

### 389 **Author Contributions**

390 Conceptualization MD, MC and JAT; Methodology, EAZ; Formal analysis, EAZ and MAD; Investigation,  
391 EAZ; Writing – Original Draft, EAZ; Writing – Review & Editing, all authors; Visualization, EAZ;  
392 Supervision, MD, MC and JAT;

### 393 **Declaration of Interests**

394 The authors declare no competing interests.

395

Journal Pre-proof

396 **Main Figure Titles and Legends**

397 **Figure 1. Visual overview of the simulated systems.** Left: visualization of the three simulated VAs (1)  
 398 ethylene, (2) desflurane, (3) methoxyflurane, and the nonimmobilizer (4) F6. Right: visualization of the  
 399 membrane system in its explicit TIP3P water box with ions and ligands omitted for clarity. P atoms highlighted  
 400 in green, POPC lipids in pink, Cholesterol in light grey, POPE in purple, POPS in dark green, PSM in bright  
 401 green. Length scale in Ångstrom reported below for reference, centered at the membrane core region.

402 **Figure 2. Distribution of the bilayer thickness ( $\delta$ ) and geometric area per lipid (gAPL).** Control simulation  
 403 vs. ethylene (A), desflurane (B), methoxyflurane (C) and F6 (D) at increasing concentrations. Marginal axes  
 404 show the individual data distributions collected in the last 750 ns of the simulations. Control simulation without  
 405 anesthetics shown in grey, 12.5% concentration in red, 25% in blue and 50% in green.

406 **Figure 3. Density distributions of lipid headgroups (blue), glycerol backbone (red), lipid tails (green) and**  
 407 **anesthetics (black).** (A) control simulation, (B) with 50% ethylene, (C) with 50% desflurane, (D) with 50%  
 408 methoxyflurane and (E) with 50% F6. Shaded colors represent 95% confidence intervals.

409 **Figure 4. Molal concentration of the four simulated ligands inside the bilayer.** Concentrations calculated  
 410 as number of moles of anesthetic per kilogram of membrane. Error bars on the histograms represent the error  
 411 estimate after block averaging.

412 **Figure 5. Lipid tail order parameters for POPC sn1 (top row) and sn2 (bottom row) chains, with different**  
 413 **ligands.** (A) and (E) ethylene; (B) and (F) desflurane; (C) and (G) methoxyflurane; (D) and (H) F6. For the  
 414 corresponding data for POPE, POPS and PSM see Supplementary Information. Shaded intervals correspond  
 415 to 95% confidence intervals.

416 **Figure 6. Effect of ligands on membrane stiffness.** (A) Bilayer bending modulus in kT units for the different  
 417 systems. Control system represented as 0% ligand concentration. Error bars represent the error estimate after  
 418 block averaging, omitted when smaller than the datapoint for clarity. (B) Correlation between anesthetic  
 419 lipophilicity (in terms of the logarithm of the octanol/water partition coefficient,  $\log(K_{o/w})$ ) and the decrease in  
 420 membrane bending modulus in kT units,  $\Delta K_c$ . Error bars represent the error estimate after block averaging,  
 421 omitted when smaller than the datapoint for clarity.

422 **Main Tables and corresponding titles and legends**

423 **Table 1.** Average geometrical Area per lipid, bilayer thickness and frequency of water permeation for all  
 424 simulated systems. 95% confidence intervals are reported in square brackets for block-averaged quantities.

System	gAPL [ $\text{\AA}^2$ ]	Bilayer Thickness ( $\delta$ ) [ $\text{\AA}$ ]	Water permeation frequency [H <sub>2</sub> O/ $\mu$ s]
C	42.89 [42.83 – 42.95]	46.85 [46.81 – 46.89]	16
<b>E12.5</b>	43.40 [43.36 – 43.44]	46.77 [46.71 – 46.83]	40
<b>E25</b>	43.90 [43.80 – 44.00]	46.74 [46.68 – 46.80]	37
<b>E50</b>	45.16 [45.12 – 45.20]	46.52 [46.46 – 46.58]	112
<b>D12.5</b>	44.93 [44.81 – 45.05]	46.17 [46.03 – 46.31]	75
<b>D25</b>	46.47 [46.41 – 46.53]	45.91 [45.89 – 45.93]	163
<b>D50</b>	48.18 [46.49 – 49.87]	45.67 [45.45 – 45.89]	285
<b>M12.5</b>	45.12 [45.08 – 45.16]	45.88 [45.87 – 45.89]	64
<b>M25</b>	46.86 [46.83 – 46.89]	45.40 [45.38 – 45.42]	160
<b>M50</b>	48.53 [46.92 – 50.14]	45.16 [44.89 – 45.43]	391
<b>F6 12.5</b>	44.95 [44.81 – 45.09]	45.97 [45.89 – 46.05]	93

<b>F6 25</b>	46.85 [46.65 – 47.05]	45.39 [45.28 – 45.50]	206
<b>F6 50</b>	46.44 [45.30 – 47.58]	45.52 [45.09 – 45.95]	155

425

426 Table 2. Bilayer bending modulus  $K_c$  in kT units and reduction of  $K_c$  with respect to control simulation,  $\Delta K_c$ ,  
 427 for each simulated system. 95% confidence intervals reported in square brackets.

<b>System</b>	<b><math>K_c</math> [kT]</b>	<b><math>\Delta K_c</math></b>
<b>C</b>	88.80 [87.16 – 90.44]	--
<b>E12.5</b>	86.94 [84.42 – 89.44]	1.86
<b>E25</b>	86.60 [85.14 – 88.06]	2.20
<b>E50</b>	75.20 [73.98 – 76.42]	13.60
<b>D12.5</b>	78.14 [76.94 – 79.32]	10.66
<b>D25</b>	70.34 [68.82 – 71.84]	18.46
<b>D50</b>	63.60 [59.06 – 68.14]	25.20
<b>M12.5</b>	71.54 [69.92 – 73.14]	17.26
<b>M25</b>	64.86 [64.58 – 65.14]	23.94
<b>M50</b>	63.66 [60.04 – 67.30]	25.14
<b>F6 12.5</b>	78.33 [76.85 – 79.82]	10.47
<b>F6 25</b>	70.87 [69.94 – 71.80]	17.93
<b>F6 50</b>	71.07 [66.61 – 75.52]	17.73

428

429 **STAR Methods**430 **Resource Availability**431 **Lead Contact**

432 Further information and requests for resources should be directed to Lead Contact, prof. Marco A. Deriu  
 433 (marco.deri@polito.it).

434 **Materials Availability**

435 This study did not generate any novel reagents and all materials used in this study are reported either the  
 436 main text or in the Supplemental Information.

437 **Data and Code Availability**

- 438
- All data reported in this paper will be shared by the lead contact upon request.
  - This paper does not report original code.
  - Any additional information required to reanalyze the data reported in this paper is available from the  
 441 lead contact upon request.

442 **Method Details**443 **System Setup**

444 To overcome the intrinsic simplifications of single-component bilayers, and to account for the presence of  
 445 cholesterol, which has a well-documented ordering effect on membranes (Róg et al., 2009) with profound  
 446 consequences on their mechanical properties (Leftin et al., 2014; Needham and Nunn, 1990), we chose to  
 447 simulate a composite asymmetrical lipid patch representative of the mammalian cell membrane, as first  
 448 described by Zachowski (1993) (Zachowski, 1993) and employed in computational studies by Klähn and  
 449 Zacharias (Klähn and Zacharias, 2013) and, more recently, Shahane et al. (Shahane et al., 2019b), composed  
 450 of POPC (1,2-palmitoyl-oleoyl-sn-glycero-3-phosphocholine), POPE (1-Palmitoyl-2-oleoyl-sn-glycero-3-  
 451 phosphoethanolamine), POPS (1,2-palmitoyl-oleoyl-sn-glycero-3-phosphoserine), PSM  
 452 (palmitoylsphingomyelin) and Cholesterol (CHOL). The detailed amounts of the lipids in the two leaflets are  
 453 reported in the following table:

454 *Table. Number of different lipid molecules in the two leaflets of the model mammalian membrane.*

Lipid	Inner Leaflet	Outer Leaflet	Total
<b>POPC</b>	40	106	146
<b>POPE</b>	132	34	166
<b>POPS</b>	82	8	90
<b>PSM</b>	10	116	126
<b>CHOL</b>	136	136	272
<b>Total</b>	<b>400</b>	<b>400</b>	<b>800</b>

455

456 Bilayer systems were assembled using the Membrane Builder (Jo et al., 2009, 2007; Wu et al., 2014) tool of  
 457 CHARMM-GUI (Jo et al., 2008), with a fixed number of 50 TIP3P waters per lipid to ensure adequate lipid  
 458 hydration even at higher ligand concentrations, and a physiological NaCl concentration of 0.15M. In addition  
 459 to the control simulation without any anesthetic, different systems were set up by randomly inserting  
 460 desflurane, methoxyflurane, ethylene and F6 (1,2-Dichlorohexafluorocyclobutane) respectively in the  
 461 surrounding aqueous solvent at 12.5%, 25% and 50% anesthetic/lipid molar ratios, for a total of 10 simulated  
 462 systems, using the *insert-molecules* tool of GROMACS 2020.4 (Abraham et al., 2015). The higher  
 463 concentrations (25%, 50%), while not intended to be representative of clinical concentrations, were included  
 464 to enhance the sampling of the lipid-anesthetic interaction and to accelerate ligand partitioning, as seen in  
 465 previously published studies (Arvayo-Zatarain et al., 2019; Koubi et al., 2000; Mojumdar and Lyubartsev,  
 466 2010). The 12.5% concentration on the other hand is more representative of clinical scenarios, with the molar  
 467 ratio of e.g. Halothane at MAC being in the range of 5% (McCarthy et al., 2017) to 14% (Franks and Lieb,  
 468 1979). The detailed composition of each simulated system is reported in the table below.

469 *Table. Components of each simulation system*

System	Short Name	Lipids	Water molecules	Cl <sup>-</sup> ions	Na <sup>+</sup> ions	VA molecules	Total Molecules
<b>Control</b>	<b>C</b>	800	40000	96	186	0	41082
<b>Ethylene 12.5%</b>	<b>E12.5</b>	800	39754	96	186	100	40936

<b>Ethylene 25%</b>	<b>E25</b>	800	39527	96	186	200	40809
<b>Ethylene 50%</b>	<b>E50</b>	800	39062	96	186	400	40544
<b>Desflurane 12.5%</b>	<b>D12.5</b>	800	39414	96	186	100	40596
<b>Desflurane 25%</b>	<b>D25</b>	800	38892	96	186	200	40174
<b>Desflurane 50%</b>	<b>D50</b>	800	37749	96	186	400	39231
<b>Methoxyflurane 12.5%</b>	<b>M12.5</b>	800	39210	96	186	100	40392
<b>Methoxyflurane 25%</b>	<b>M25</b>	800	38484	96	186	200	39766
<b>Methoxyflurane 50%</b>	<b>M50</b>	800	36755	96	186	400	38237
<b>F6 12.5%</b>	<b>F6 12.5</b>	800	39149	96	186	100	40331
<b>F6 25%</b>	<b>F6 25</b>	800	38381	96	186	200	39663
<b>F6 50%</b>	<b>F6 50</b>	800	36486	96	186	400	37968

470

471 *Simulation Protocol*

472 Simulations were carried out in GROMACS 2020.4 (Abraham et al., 2015) using the CHARMM36 force field  
473 (Klauda et al., 2010), which is well-validated for membrane simulations over a wide range of lipid  
474 compositions (Zhuang et al., 2014), according to the following protocol: after an initial 5000-step energy  
475 minimization, systems were equilibrated stepwise with gradually decreasing harmonic restraints (from 1000  
476 to  $0 \text{ kJ} \times \text{mol}^{-1} \times \text{nm}^{-1}$ ), first in the NVT ensemble for 250 ps with a conservative timestep of 1 fs, using the  
477 Berendsen thermostat with a coupling time constant of 1 ps and a reference temperature of 303.15K, which is  
478 above the phase-transition temperature for the studied lipid mixture, and subsequently in the NPT ensemble  
479 for 125 ps with the same 1 fs timestep, followed by a further simulation of 375 ps with a 2 fs timestep, using  
480 the Berendsen thermostat with the same parameters as before and the Berendsen barostat (Berendsen et al.,  
481 1984) with semi-isotropic pressure coupling at 1 atm with a coupling time constant of 5 ps. Overall, systems  
482 underwent 750 ps of equilibration, and were subsequently simulated for production runs for a total of 1  $\mu\text{s}$  each  
483 in the NPT ensemble, using the Nosé-Hoover thermostat (Nosé, 1998) with a time constant of 1 ps and a  
484 reference temperature of 303.15K, and the Parrinello-Rahman barostat (Parrinello and Rahman, 1981), with  
485 semi-isotropic pressure coupling at 1 atm with a time constant of 5 ps. Bonds involving hydrogens were  
486 constrained using the LINCS algorithm (Hess et al., 1997), while the Particle Mesh Ewald (PME) algorithm  
487 (Ewald, 1921) was used for electrostatics, with a cutoff radius of 1.2 nm, and a cutoff of 1.2 nm was used for  
488 Van der Waals interactions, with a force-switch modifier from 1.0 to 1.2 nm. The first 250 ns of the production  
489 MD runs were regarded as additional structural equilibration, while the remaining 750 ns were used for the  
490 subsequent analyses described below, in line with previous literature regarding the computational simulation  
491 of biological lipid bilayers (Shahane et al., 2019a, 2019b). Properties were sampled every 200 ps, unless  
492 otherwise specified. Molecular visualizations were generated using the VMD software package (Humphrey et  
493 al., 1996).

494 *Structural Analyses*

495 Geometric Area-per-Lipid (gAPL), Bilayer Thickness ( $\delta$ ) and water permeation were calculated using the  
496 MDAnalysis (Michaud-Agrawal et al., 2011) library for Python (Van Rossum and Drake, 2009). Briefly, the  
497 gAPL was calculated as the  $xy$  area of the simulation box divided by the number of lipids in each membrane

498 leaflet (N=400) and is reported in Å<sup>2</sup>. To calculate the bilayer thickness, the position of all P atoms of each  
 499 leaflet was extracted and their average z coordinate calculated for each leaflet. Bilayer thickness was calculated  
 500 as the distance between the avg. z coordinates the P atom cloud. Water permeation events were calculated by  
 501 tracking individual water molecules throughout the simulation. Density distribution profiles along the z  
 502 coordinate were calculated using the *gmx density* tool. Acyl chain deuterium order parameters, S<sub>CD</sub>, for the sn1  
 503 and sn2 chains of each lipid were calculated to directly quantify structural effects on the packing of the  
 504 membranes' hydrophobic core. Order parameters were calculated following equation (1), using the *gmx order*  
 505 tool:

$$506 \quad S_{CD} = \frac{1}{2} \langle 3 \cos^2 \theta - 1 \rangle \quad (1)$$

507 where  $\theta$  is defined as the angle between the bilayer normal and the vector C-D between the given carbon atom  
 508 and the bound hydrogen atom, as sampled from the equilibrium MD simulations (Piggot et al., 2017).  
 509 Unsaturated lipid chains were accounted for following the methodology described in Pluhackova et al.  
 510 (Pluhackova et al., 2016).

511 To quantify the tendency of ligands to partition inside the bilayer, which can bear profound consequences on  
 512 protein-ligand interaction affinity and kinetics on transmembrane protein targets, the ligand molal  
 513 concentration inside the lipid bilayer was calculated as follows. MDAnalysis was used to extract the number  
 514 of ligand molecules whose center-of-mass z coordinate lied between the two P-atom point clouds, i.e. between  
 515 the two layers delimiting each leaflet's boundary. These ligands were regarded as being embedded inside the  
 516 membrane. The remainder of the ligands was considered outside of the membrane. The molality of the  
 517 anesthetics inside the membrane was calculated as number of moles of embedded ligands divided by the total  
 518 weight of the membrane in kg.

519 To calculate the bilayer bending modulus, K<sub>c</sub>, for each simulated system, the methodology proposed by  
 520 Khelashvili and colleagues (Khelashvili et al., 2013) was employed, leveraging on the relationship between  
 521 the splay modulus,  $\chi_{12}$ , and the macroscopic bending modulus: in this approach, an improved ability of adjacent  
 522 lipids to change the reciprocal orientation of their hydrophobic tails with respect to the local membrane normal,  
 523 which is quantified by their splay angle ( $\alpha$ ), is associated to a decreased membrane bending rigidity. Briefly,  
 524 this approach first calculates the Potential of Mean Force (PMF) of the distribution of splay angles sampled  
 525 during equilibrium MD simulations, normalized with respect to the probability distribution of a non-interacting  
 526 particle system (Khelashvili et al., 2010), denoted here P<sub>0</sub>( $\alpha$ ), as shown in equation (2):

$$527 \quad PMF(\alpha) = -k_B T \ln \frac{P(\alpha)}{P_0(\alpha)} \quad (2)$$

528 where T represents the system temperature and k<sub>B</sub> the Boltzmann constant. The overall splay modulus, which  
 529 is linked to the bilayer bending modulus as:

$$530 \quad K_c = 2k_m = 2\chi_{12} \quad (3)$$

531 can be calculated by means of a quadratic fit of the PMF obtained from Eq. (2) (Fošnarič et al., 2006; Watson  
532 et al., 2011).

533 In the present work, we employed the python implementation previously demonstrated by Johner et al. (Johner  
534 et al., 2016) to first extend the trajectories to neighboring periodic images, followed by wrapping the trajectory  
535 around the central unit cell and re-aligning. Finally, the provided python modules were used to calculate the  
536 tilt and splay angle distributions for all lipids and subsequently extract the membrane elastic properties of  
537 interest following the above-mentioned methodology. We refer to (Johner et al., 2016) and references therein  
538 for a more complete theoretical background of the methodology and details on the python implementation  
539 relying on the OpenStructure (Biasini et al., 2013) toolkit.

#### 540 **Quantification and statistical Analysis**

541 For a more accurate estimation of the error of the sampled properties (Flyvbjerg and Petersen, 1989; Grossfield  
542 et al., 2019; Grossfield and Zuckerman, 2009; Nicholls, 2014), the equilibrium part of the MD simulations (i.e.  
543 the last 750 ns) was further divided into 250-ns long trajectory blocks, in line with previous literature reporting  
544 findings in  $\mu$ s-long MD simulations of complex lipid membranes (Shahane et al., 2019a, 2019b). First, the  
545 block average of each structural property was calculated for each block as the arithmetic mean of the data  
546 points of the given property  $p$  within the block:

$$547 \quad \bar{\mu}_j = \frac{1}{N_b} \sum_{i=1}^{N_b} p_i \quad (4)$$

548 where  $\bar{\mu}_j$  denotes the mean within the  $j$ -th block of property  $p$  and  $N_b$  is the number of samples composing the  
549  $j$ -th block. The final estimate of the ensemble average  $\langle \mu \rangle$  of the given property  $p$  is given by the arithmetic  
550 mean of the block averages:

$$551 \quad \langle \mu \rangle = \frac{1}{n} \sum_{j=1}^n \bar{\mu}_j \quad (5)$$

552 where  $n$  is the total number of blocks. Then, the experimental standard deviation of the mean,  $\bar{\sigma}_\mu$ , of each  
553 property was calculated as:

$$554 \quad \bar{\sigma}_\mu = \sqrt{\frac{\sum_{j=1}^n (\bar{\mu}_j - \langle \mu \rangle)^2}{n - 1}} \quad (6)$$

555 where  $\bar{\mu}_j$  is the arithmetic mean of a given property over the  $j$ -th block and  $n$  is the number of blocks. Finally,  
556 the estimate of the standard deviation is given by:

$$557 \quad \sigma_\mu = \frac{\bar{\sigma}_\mu}{n} \quad (7)$$

558 This quantity is the reported standard deviation, represented as error bars on the plots, and was also used to  
559 calculate 95% confidence intervals which are reported throughout the text and in shaded colors on the plots,  
560 unless where explicitly specified.

Journal Pre-proof

561 **References**

- 562 Abraham, M.J., Murtola, T., Schulz, R., Páll, S., Smith, J.C., Hess, B., Lindah, E., 2015. Gromacs: High  
563 performance molecular simulations through multi-level parallelism from laptops to supercomputers.  
564 SoftwareX 1–2, 19–25. <https://doi.org/10.1016/j.softx.2015.06.001>
- 565 Allen, J.A., Halverson-Tamboli, R.A., Rasenick, M.M., 2006. Lipid raft microdomains and neurotransmitter  
566 signalling. *Nat. Rev. Neurosci.* 2007 82 8, 128–140. <https://doi.org/10.1038/nrn2059>
- 567 Arvayo-Zatarain, J.A., Favela-Rosales, F., Contreras-Aburto, C., Urrutia-Bañuelos, E., Maldonado, A., 2019.  
568 Molecular dynamics simulation study of the effect of halothane on mixed DPPC/DPPE phospholipid  
569 membranes. *J. Mol. Model.* 25, 1–10. <https://doi.org/10.1007/s00894-018-3890-6>
- 570 Bennett, W.F.D., MacCallum, J.L., Hinner, M.J., Marrink, S.J., Tieleman, D.P., 2009. Molecular view of  
571 cholesterol flip-flop and chemical potential in different membrane environments. *J. Am. Chem. Soc.*  
572 131, 12714–12720. [https://doi.org/10.1021/JA903529F/SUPPL\\_FILE/JA903529F\\_SI\\_001.PDF](https://doi.org/10.1021/JA903529F/SUPPL_FILE/JA903529F_SI_001.PDF)
- 573 Berendsen, H.J.C., Postma, J.P.M., Van Gunsteren, W.F., DiNola, A., Haak, J.R., 1984. Molecular dynamics  
574 with coupling to an external bath. *J. Chem. Phys.* 81.
- 575 Bertaccini, E.J., 2010. The molecular mechanisms of anesthetic action: Updates and cutting edge  
576 developments from the field of molecular modeling. *Pharmaceuticals.*  
577 <https://doi.org/10.3390/ph3072178>
- 578 Bertaccini, E.J., Yoluk, O., Lindahl, E.R., Trudell, J.R., 2013. Assessment of Homology Templates and an  
579 Anesthetic Binding Site within the  $\gamma$ -Aminobutyric Acid Receptor. *Anesthesiology* 119, 1087–1095.  
580 <https://doi.org/10.1097/ALN.0B013E31829E47E3>
- 581 Biasini, M., Schmidt, T., Bienert, S., Mariani, V., Studer, G., Haas, J., Johner, N., Schenk, A.D., Philippsen,  
582 A., Schwede, T., 2013. OpenStructure: An integrated software framework for computational structural  
583 biology. *Acta Crystallogr. Sect. D Biol. Crystallogr.* 69, 701–709.  
584 <https://doi.org/10.1107/S0907444913007051/IC5090SUP2.TXT>
- 585 Campagna, J.A., Miller, K.W., Forman, S.A., 2003. Mechanisms of Actions of Inhaled Anesthetics. *N. Engl.*  
586 *J. Med.* 348, 2110–2124. <https://doi.org/10.1056/nejmra021261>
- 587 Cantor, R.S., 1999. Lipid Composition and the Lateral Pressure Profile in Bilayers. *Biophys. J.* 76, 2625–  
588 2639. [https://doi.org/10.1016/S0006-3495\(99\)77415-1](https://doi.org/10.1016/S0006-3495(99)77415-1)
- 589 Cantor, R.S., 1997. The Lateral Pressure Profile in Membranes: A Physical Mechanism of General  
590 Anesthesia. *Biochemistry* 36, 2339–2344. <https://doi.org/10.1021/BI9627323>
- 591 Christophe Chipot, †,§, Michael A. Wilson, †,‡ and, Andrew Pohorille\*, †,‡, 1997. Interactions of  
592 Anesthetics with the Water–Hexane Interface. A Molecular Dynamics Study. *J. Phys. Chem. B* 101,  
593 782–791. <https://doi.org/10.1021/JP961513O>

- 594 De Planque, M.R.R., Killian, J.A., 2003. Protein-lipid interactions studied with designed transmembrane  
595 peptides: Role of hydrophobic matching and interfacial anchoring (Review). *Mol. Membr. Biol.* 20,  
596 271–284. <https://doi.org/10.1080/09687680310001605352>
- 597 Dickson, C.J., Madej, B.D., Skjevik, Å.A., Betz, R.M., Teigen, K., Gould, I.R., Walker, R.C., 2014. Lipid14:  
598 The amber lipid force field. *J. Chem. Theory Comput.* 10, 865–879.  
599 <https://doi.org/10.1021/CT4010307>
- 600 Dickson, C.J., Rosso, L., Betz, R.M., Walker, R.C., Gould, I.R., 2012. GAFFlipid: A General Amber Force  
601 Field for the accurate molecular dynamics simulation of phospholipid. *Soft Matter* 8, 9617–9627.  
602 <https://doi.org/10.1039/C2SM26007G>
- 603 Dumas, F., Lebrun, M.C., Tocanne, J.F., 1999. Is the protein/lipid hydrophobic matching principle relevant  
604 to membrane organization and functions? *FEBS Lett.* 458, 271–277. [https://doi.org/10.1016/S0014-](https://doi.org/10.1016/S0014-5793(99)01148-5)  
605 [5793\(99\)01148-5](https://doi.org/10.1016/S0014-5793(99)01148-5)
- 606 Eger, E.I., Halsey, M.J., Koblin, D.D., Laster, M.J., Ionescu, P., Königsberger, K., Fan, R., Nguyen, B. V.,  
607 Hudlicky, T., 2001. The convulsant and anesthetic properties of cis-trans isomers of 1,2-  
608 dichlorohexafluorocyclobutane and 1,2-dichloroethylene. *Anesth. Analg.* 93, 922–927.  
609 <https://doi.org/10.1097/00000539-200110000-00025>
- 610 Ewald, P., 1921. Die Berechnung optischer und elektrostatischer Gitterpotentiale. *Ann. Phys.*
- 611 Flyvbjerg, H., Petersen, H.G., 1989. Error estimates on averages of correlated data. *J. Chem. Phys.* 91, 461–  
612 466. <https://doi.org/10.1063/1.457480>
- 613 Fošnarič, M., Iglič, A., May, S., 2006. Influence of rigid inclusions on the bending elasticity of a lipid  
614 membrane. *Phys. Rev. E* 74, 051503. <https://doi.org/10.1103/PhysRevE.74.051503>
- 615 Franks, N.P., Lieb, W.R., 1994. Molecular and cellular mechanisms of general anaesthesia. *Nat.* 1994  
616 3676464 367, 607–614. <https://doi.org/10.1038/367607a0>
- 617 Franks, N.P., Lieb, W.R., 1984. Do general anaesthetics act by competitive binding to specific receptors?  
618 *Nat.* 1984 3105978 310, 599–601. <https://doi.org/10.1038/310599a0>
- 619 Franks, N.P., Lieb, W.R., 1979. The structure of lipid bilayers and the effects of general anaesthetics: An X-  
620 ray and neutron diffraction study. *J. Mol. Biol.* 133, 469–500. [https://doi.org/10.1016/0022-](https://doi.org/10.1016/0022-2836(79)90403-0)  
621 [2836\(79\)90403-0](https://doi.org/10.1016/0022-2836(79)90403-0)
- 622 Grasso, G., Muscat, S., Rebella, M., Morbiducci, U., Audenino, A., Danani, A., Deriu, M.A., 2018. Cell  
623 penetrating peptide modulation of membrane biomechanics by Molecular dynamics. *J. Biomech.* 73,  
624 137–144. <https://doi.org/10.1016/j.jbiomech.2018.03.036>
- 625 Gray, E., Karlake, J., Machta, B.B., Veatch, S.L., 2013. Liquid general anesthetics lower critical

- 626 temperatures in plasma membrane vesicles. *Biophys. J.* 105, 2751–2759.  
627 <https://doi.org/10.1016/j.bpj.2013.11.005>
- 628 Grossfield, A., Patrone, P.N., Roe, D.R., Schultz, A.J., Siderius, D., Zuckerman, D.M., 2019. Best Practices  
629 for Quantification of Uncertainty and Sampling Quality in Molecular Simulations [Article v1.0]. *Living*  
630 *J. Comput. Mol. Sci.* 1, 1–24. <https://doi.org/10.33011/livecoms.1.1.5067>
- 631 Grossfield, A., Zuckerman, D.M., 2009. Chapter 2 Quantifying Uncertainty and Sampling Quality in  
632 Biomolecular Simulations. *Annu. Rep. Comput. Chem.* [https://doi.org/10.1016/S1574-1400\(09\)00502-](https://doi.org/10.1016/S1574-1400(09)00502-7)  
633 7
- 634 Herold, K.F., Hemmings, H.C., 2012. Sodium channels as targets for volatile anesthetics. *Front. Pharmacol.*  
635 3 MAR, 50. <https://doi.org/10.3389/fphar.2012.00050>
- 636 Herold, K.F., Sanford, R.L., Lee, W., Andersen, O.S., Hemmings, H.C., 2017. Clinical concentrations of  
637 chemically diverse general anesthetics minimally affect lipid bilayer properties. *Proc. Natl. Acad. Sci.*  
638 U. S. A. 114, 3109–3114. <https://doi.org/10.1073/pnas.1611717114>
- 639 Hess, B., Bekker, H., Berendsen, H.J.C., Fraaije, J.G.E.M., 1997. LINCS: A Linear Constraint Solver for  
640 Molecular Simulations. *J Comput Chem* 18, 14631472. [https://doi.org/10.1002/\(SICI\)1096-](https://doi.org/10.1002/(SICI)1096-987X(199709)18:12)  
641 987X(199709)18:12
- 642 Hofsäß, C., Lindahl, E., Edholm, O., 2003. Molecular Dynamics Simulations of Phospholipid Bilayers with  
643 Cholesterol. *Biophys. J.* 84, 2192. [https://doi.org/10.1016/S0006-3495\(03\)75025-5](https://doi.org/10.1016/S0006-3495(03)75025-5)
- 644 Huang, P., Bertaccini, E., 1995. Molecular dynamics simulation of anesthetic-phospholipid bilayer  
645 interactions. *J. Biomol. Struct. Dyn.* 12, 725–754. <https://doi.org/10.1080/07391102.1995.10508773>
- 646 Humphrey, W., Dalke, A., Schulten, K., 1996. VMD: visual molecular dynamics. *J. Mol. Graph.* 14, 27-  
647 28,33-38. [https://doi.org/10.1016/0263-7855\(96\)00018-5](https://doi.org/10.1016/0263-7855(96)00018-5)
- 648 Ingólfsson, H.I., Carpenter, T.S., Bhatia, H., Bremer, P.T., Marrink, S.J., Lightstone, F.C., 2017.  
649 Computational Lipidomics of the Neuronal Plasma Membrane. *Biophys. J.* 113, 2271–2280.  
650 <https://doi.org/10.1016/j.bpj.2017.10.017>
- 651 Jämbeck, J.P.M., Lyubartsev, A.P., 2012. Derivation and Systematic Validation of a Refined All-Atom Force  
652 Field for Phosphatidylcholine Lipids. *J. Phys. Chem. B* 116, 3164–3179.  
653 <https://doi.org/10.1021/jp212503e>
- 654 Jo, S., Kim, T., Im, W., 2007. Automated Builder and Database of Protein/Membrane Complexes for  
655 Molecular Dynamics Simulations. *PLoS One* 2, e880. <https://doi.org/10.1371/journal.pone.0000880>
- 656 Jo, S., Kim, T., Iyer, V.G., Im, W., 2008. CHARMM-GUI: A web-based graphical user interface for  
657 CHARMM. *J. Comput. Chem.* 29, 1859–1865. <https://doi.org/10.1002/jcc.20945>

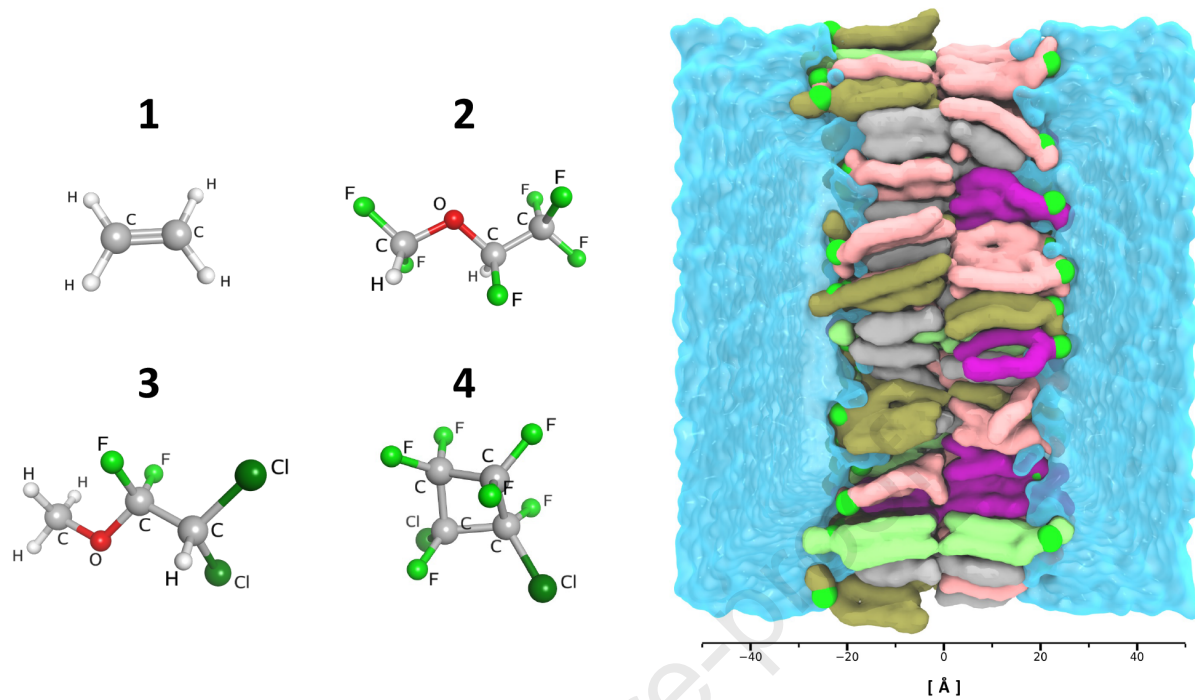
- 658 Jo, S., Lim, J.B., Klauda, J.B., Im, W., 2009. CHARMM-GUI Membrane Builder for Mixed Bilayers and Its  
659 Application to Yeast Membranes. *Biophys. J.* 97, 50–58. <https://doi.org/10.1016/j.bpj.2009.04.013>
- 660 John Mihic, S., Ye, Q., Wick, M.J., Koltchine, V. V., Krasowski, M.D., Finn, S.E., Mascia, M.P., Fernando  
661 Valenzuela, C., Hanson, K.K., Greenblatt, E.P., Adron Harris, R., Harrison, N.L., 1997. Sites of alcohol  
662 and volatile anaesthetic action on GABA(A) and glycine receptors. *Nature* 389, 385–389.  
663 <https://doi.org/10.1038/38738>
- 664 Johner, N., Harries, D., Khelashvili, G., 2016. Implementation of a methodology for determining elastic  
665 properties of lipid assemblies from molecular dynamics simulations. *BMC Bioinformatics* 17, 1–11.  
666 <https://doi.org/10.1186/s12859-016-1003-z>
- 667 Khelashvili, G., Kollmitzer, B., Heftberger, P., Pabst, G., Harries, D., 2013. Calculating the bending modulus  
668 for multicomponent lipid membranes in different thermodynamic phases. *J. Chem. Theory Comput.* 9,  
669 3866–3871. <https://doi.org/10.1021/ct400492e>
- 670 Khelashvili, G., Pabst, G., Harries, D., 2010. Cholesterol Orientation and Tilt Modulus in DMPC Bilayers. *J.*  
671 *Phys. Chem. B* 114, 7524–7534. <https://doi.org/10.1021/jp101889k>
- 672 Klähn, M., Zacharias, M., 2013. Transformations in plasma membranes of cancerous cells and resulting  
673 consequences for cation insertion studied with molecular dynamics. *Phys. Chem. Chem. Phys.* 15,  
674 14427–14441. <https://doi.org/10.1039/c3cp52085d>
- 675 Klauda, J.B., Venable, R.M., Freites, J.A., O'Connor, J.W., Tobias, D.J., Mondragon-Ramirez, C.,  
676 Vorobyov, I., MacKerell, A.D., Pastor, R.W., 2010. Update of the CHARMM All-Atom Additive  
677 Force Field for Lipids: Validation on Six Lipid Types. *J. Phys. Chem. B* 114, 7830–7843.  
678 <https://doi.org/10.1021/jp101759q>
- 679 Koblin, D.D., Eger, E.I., Johnson, B.H., Collins, P., Terrell, R.C., Speers, L., 1981. Are convulsant gases  
680 also anesthetics? *Anesth. Analg.* 60, 464–470. <https://doi.org/10.1213/00000539-198107000-00002>
- 681 Koubi, L., Tarek, M., Klein, M.L., Scharf, D., 2000. Distribution of Halothane in a  
682 Dipalmitoylphosphatidylcholine Bilayer from Molecular Dynamics Calculations. *Biophys. J.* 78, 800–  
683 811. [https://doi.org/10.1016/S0006-3495\(00\)76637-9](https://doi.org/10.1016/S0006-3495(00)76637-9)
- 684 Lee, A.G., 1976. Model for action of local anaesthetics. *Nat.* 1976 2625569 262, 545–548.  
685 <https://doi.org/10.1038/262545a0>
- 686 Leftin, A., Molugu, T.R., Job, C., Beyer, K., Brown, M.F., 2014. Area per Lipid and Cholesterol Interactions  
687 in Membranes from Separated Local-Field <sup>13</sup>C NMR Spectroscopy. *Biophys. J.* 107, 2274–2286.  
688 <https://doi.org/10.1016/J.BPJ.2014.07.044>
- 689 Lerner, R.A., 1997. A hypothesis about the endogenous analogue of general anesthesia. *Proc. Natl. Acad.*  
690 *Sci.* 94, 13375–13377. <https://doi.org/10.1073/PNAS.94.25.13375>

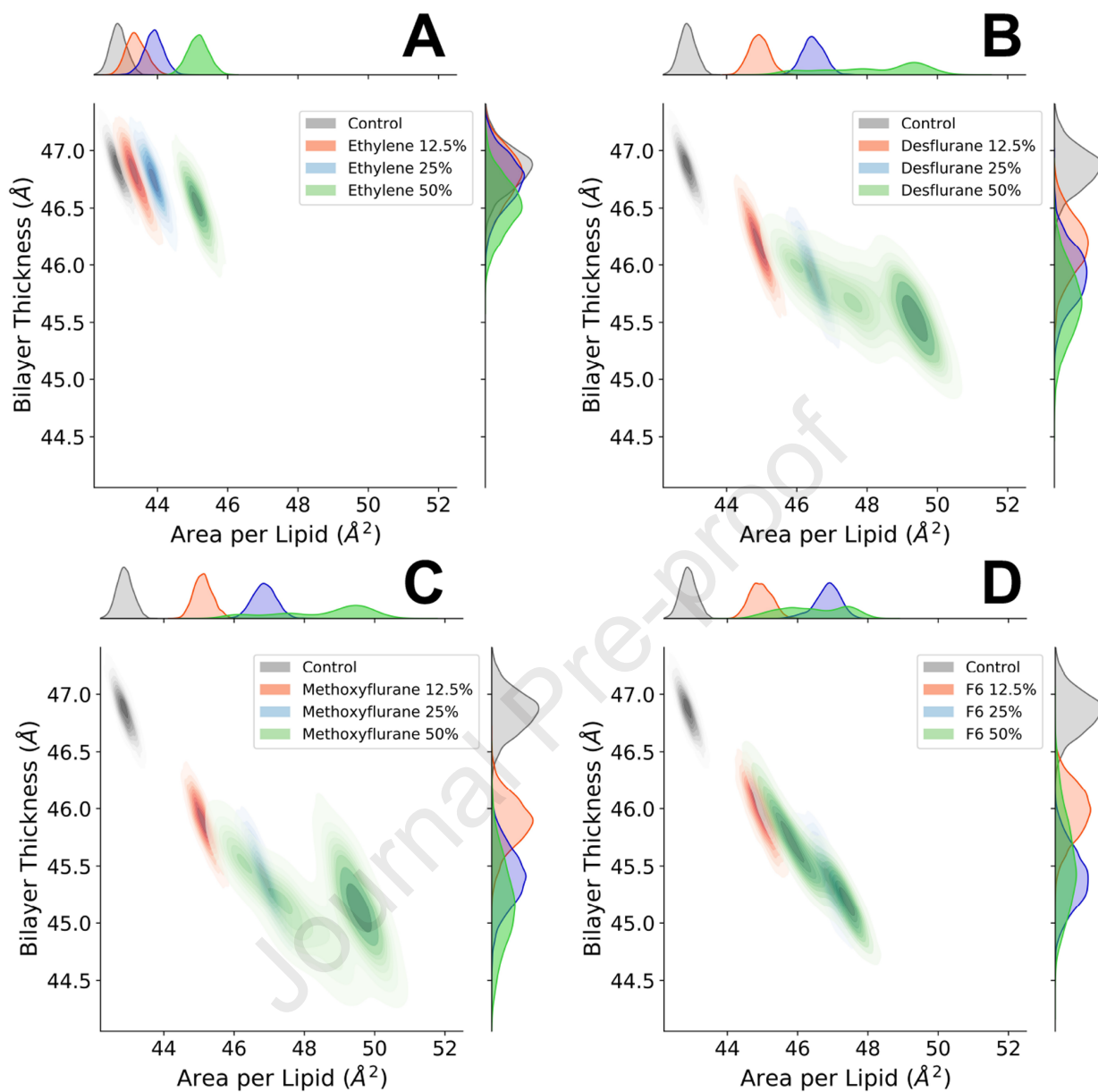
- 691 Levental, I., Grzybek, M., Simons, K., 2011. Raft domains of variable properties and compositions in plasma  
692 membrane vesicles. *Proc. Natl. Acad. Sci.* 108, 11411–11416.  
693 <https://doi.org/10.1073/PNAS.1105996108>
- 694 Li, L.B., Vorobyov, I., Allen, T.W., 2012. The role of membrane thickness in charged protein–lipid  
695 interactions. *Biochim. Biophys. Acta - Biomembr.* 1818, 135–145.  
696 <https://doi.org/10.1016/J.BBAMEM.2011.10.026>
- 697 Lingwood, D., Simons, K., 2010. Lipid rafts as a membrane-organizing principle. *Science* (80-. ). 327, 46–  
698 50. [https://doi.org/10.1126/SCIENCE.1174621/ASSET/2C0E3756-BFCD-450C-8749-  
699 7EE77CABA75A/ASSETS/GRAPHIC/327\\_46\\_F3.JPEG](https://doi.org/10.1126/SCIENCE.1174621/ASSET/2C0E3756-BFCD-450C-8749-7EE77CABA75A/ASSETS/GRAPHIC/327_46_F3.JPEG)
- 700 Mascia, M.P., Trudell, J.R., Harris, R.A., 2000. Specific binding sites for alcohols and anesthetics on ligand-  
701 gated ion channels. *Proc. Natl. Acad. Sci.* 97, 9305–9310. <https://doi.org/10.1073/PNAS.160128797>
- 702 Maulik, P.R., Shipley, G.G., 1996. Interactions of N-stearoyl sphingomyelin with cholesterol and  
703 dipalmitoylphosphatidylcholine in bilayer membranes. *Biophys. J.* 70, 2256–2265.  
704 [https://doi.org/10.1016/S0006-3495\(96\)79791-6](https://doi.org/10.1016/S0006-3495(96)79791-6)
- 705 Mazze, R.I., 1971. Renal Dysfunction Associated With Methoxyflurane Anesthesia. *JAMA* 216, 278.  
706 <https://doi.org/10.1001/jama.1971.03180280032006>
- 707 McCarthy, N.L.C., Brooks, N.J., Tyler, A.I.I., ElGamacy, M., Welche, P.R.L., Payne, M.C., Chau, P.L.,  
708 2017. A combined X-ray scattering and simulation study of halothane in membranes at raised  
709 pressures. *Chem. Phys. Lett.* 671, 21–27. <https://doi.org/10.1016/J.CPLETT.2016.12.041>
- 710 Meyer, F. de, Smit, B., 2009. Effect of cholesterol on the structure of a phospholipid bilayer. *Proc. Natl.*  
711 *Acad. Sci.* 106, 3654–3658. <https://doi.org/10.1073/PNAS.0809959106>
- 712 Meyer, K.H., 1937. Contributions to the theory of narcosis. *Trans. Faraday Soc.* 33, 1062–1064.  
713 <https://doi.org/10.1039/TF9373301062>
- 714 Michaud-Agrawal, N., Denning, E.J., Woolf, T.B., Beckstein, O., 2011. MDAnalysis: A toolkit for the  
715 analysis of molecular dynamics simulations. *J. Comput. Chem.* 32, 2319–2327.  
716 <https://doi.org/10.1002/jcc.21787>
- 717 Miller, R.D., Wahrenbrock, E.A., Schroeder, C.F., Knipstein, T.W., Eger, E.I., Buechel, D.R., 1969.  
718 Ethylene--halothane anesthesia: addition or synergism? *Anesthesiology*.  
719 <https://doi.org/10.1097/00000542-196910000-00002>
- 720 Modica, P.A., Templehoff, R., White, P.F., 1990. Pro- and anticonvulsant effects of anesthetics (Part II).  
721 *Anesth. Analg.* 70, 433–444. <https://doi.org/10.1213/00000539-199004000-00016>
- 722 Mojumdar, E.H., Lyubartsev, A.P., 2010. Molecular dynamics simulations of local anesthetic articaine in a

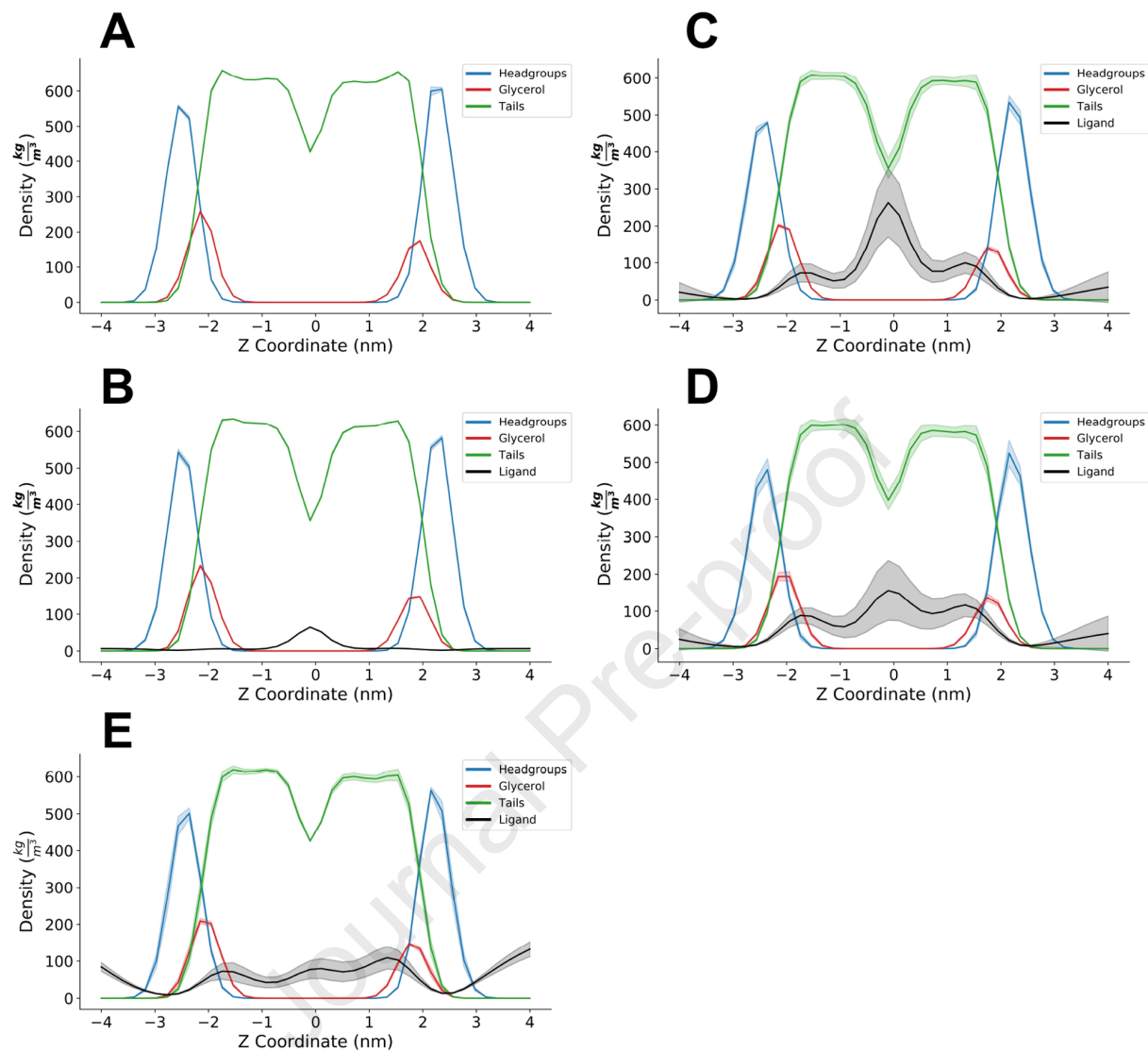
- 723 lipid bilayer. *Biophys. Chem.* 153, 27–35. <https://doi.org/10.1016/j.bpc.2010.10.001>
- 724 Moon, S., Yan, R., Kenny, S.J., Shyu, Y., Xiang, L., Li, W., Xu, K., 2017. Spectrally Resolved, Functional  
725 Super-Resolution Microscopy Reveals Nanoscale Compositional Heterogeneity in Live-Cell  
726 Membranes. *J. Am. Chem. Soc.* 139, 10944–10947.  
727 [https://doi.org/10.1021/JACS.7B03846/SUPPL\\_FILE/JA7B03846\\_SI\\_004.MPG](https://doi.org/10.1021/JACS.7B03846/SUPPL_FILE/JA7B03846_SI_004.MPG)
- 728 Mouritsen, O.G., Bloom, M., 1993. Models of Lipid-Protein Interactions in Membranes. *Annu. Rev.*  
729 *Biophys. Biomol. Struct.* 22, 145–171. <https://doi.org/10.1146/annurev.bb.22.060193.001045>
- 730 Needham, D., Nunn, R.S., 1990. Elastic deformation and failure of lipid bilayer membranes containing  
731 cholesterol. *Biophys. J.* 58, 997–1009. [https://doi.org/10.1016/S0006-3495\(90\)82444-9](https://doi.org/10.1016/S0006-3495(90)82444-9)
- 732 Nicholls, A., 2014. Confidence limits, error bars and method comparison in molecular modeling. Part 1: The  
733 calculation of confidence intervals. *J. Comput. Aided. Mol. Des.* 28, 887–918.  
734 <https://doi.org/10.1007/s10822-014-9753-z>
- 735 Nosé, S., 1998. A unified formulation of the constant temperature molecular dynamics methods. *J. Chem.*  
736 *Phys.* 81, 511. <https://doi.org/10.1063/1.447334>
- 737 Parrinello, M., Rahman, A., 1981. Polymorphic transitions in single crystals: A new molecular dynamics  
738 method. *J. Appl. Phys.* 52, 7182–7190. <https://doi.org/10.1063/1.328693>
- 739 Pavel, M.A., Petersen, E.N., Wang, H., Lerner, R.A., Hansen, S.B., 2020. Studies on the mechanism of  
740 general anesthesia. *Proc. Natl. Acad. Sci.* 117, 13757–13766. <https://doi.org/10.1073/pnas.2004259117>
- 741 Perouansky, M., Hentschke, H., Perkins, M., Pearce, R.A., 2007. Amnesic Concentrations of the  
742 Nonimmobilizer 1,2-Dichlorohexafluorocyclobutane (F6, 2N) and Isoflurane Alter Hippocampal  $\theta$   
743 Oscillations In Vivo. *Anesthesiology* 106, 1168–1176.  
744 <https://doi.org/10.1097/01.ANES.0000267600.09764.AF>
- 745 Pickholz, M., Saiz, L., Klein, M.L., 2005. Concentration effects of volatile anesthetics on the properties of  
746 model membranes: A coarse-grain approach. *Biophys. J.* 88, 1524–1534.  
747 <https://doi.org/10.1529/biophysj.104.044354>
- 748 Piggot, T.J., Allison, J.R., Sessions, R.B., Essex, J.W., 2017. On the Calculation of Acyl Chain Order  
749 Parameters from Lipid Simulations. *J. Chem. Theory Comput.* 13, 5683–5696.  
750 <https://doi.org/10.1021/acs.jctc.7b00643>
- 751 Pluhackova, K., Kirsch, S.A., Han, J., Sun, L., Jiang, Z., Unruh, T., Böckmann, R.A., 2016. A Critical  
752 Comparison of Biomembrane Force Fields: Structure and Dynamics of Model DMPC, POPC, and  
753 POPE Bilayers. *J. Phys. Chem. B* 120, 3888–3903.  
754 [https://doi.org/10.1021/ACS.JPCB.6B01870/SUPPL\\_FILE/JP6B01870\\_SI\\_001.PDF](https://doi.org/10.1021/ACS.JPCB.6B01870/SUPPL_FILE/JP6B01870_SI_001.PDF)

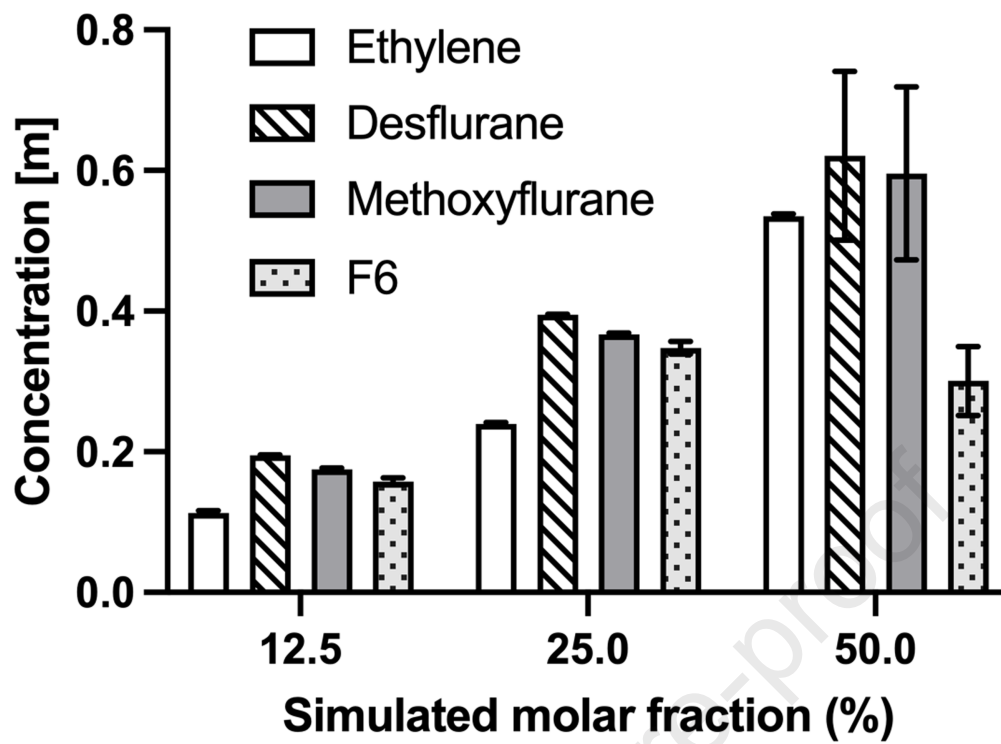
- 755 Pohorille, A., Cieplak, P., Wilson, M.A., 1996. Interactions of anesthetics with the membrane-water  
756 interface. *Chem. Phys.* 204, 337–345. [https://doi.org/10.1016/0301-0104\(95\)00292-8](https://doi.org/10.1016/0301-0104(95)00292-8)
- 757 Pohorille, A., Wilson, M.A., New, M.H., Chipot, C., 1998. Concentrations of anesthetics across the water–  
758 membrane interface; the Meyer–Overton hypothesis revisited. *Toxicol. Lett.* 100–101, 421–430.  
759 [https://doi.org/10.1016/S0378-4274\(98\)00216-1](https://doi.org/10.1016/S0378-4274(98)00216-1)
- 760 Pontes, B., Ayala, Y., Fonseca, A.C.C., Romão, L.F., Amaral, R.F., Salgado, L.T., Lima, F.R., Farina, M.,  
761 Viana, N.B., Moura-Neto, V., Nussenzveig, H.M., 2013. Membrane Elastic Properties and Cell  
762 Function. *PLoS One* 8, e67708. <https://doi.org/10.1371/journal.pone.0067708>
- 763 Riazi, S., Ibarra Moreno, C.A., 2013. *Pharmacology and Physiology for Anesthesia, Anesthesia & Analgesia.*  
764 Elsevier. <https://doi.org/10.1016/C2009-0-41712-4>
- 765 Róg, T., Pasenkiewicz-Gierula, M., Vattulainen, I., Karttunen, M., 2009. Ordering effects of cholesterol and  
766 its analogues. *Biochim. Biophys. Acta - Biomembr.* 1788, 97–121.  
767 <https://doi.org/10.1016/j.bbamem.2008.08.022>
- 768 Saedimasine, M., Montanino, A., Kleiven, S., Villa, A., 2019. Role of lipid composition on the structural  
769 and mechanical features of axonal membranes: a molecular simulation study. *Sci. Reports* 2019 9, 9,  
770 1–12. <https://doi.org/10.1038/s41598-019-44318-9>
- 771 Seeman, P., 1972. The Membrane Actions of Anesthetics and Tranquilizers. *Pharmacol. Rev.* 24, 583–655.
- 772 Shahane, G., Ding, W., Palaiokostas, M., Azevedo, H.S., Orsi, M., 2019a. Interaction of Antimicrobial  
773 Lipopeptides with Bacterial Lipid Bilayers. *J. Membr. Biol.* 252, 317–329.  
774 <https://doi.org/10.1007/s00232-019-00068-3>
- 775 Shahane, G., Ding, W., Palaiokostas, M., Orsi, M., 2019b. Physical properties of model biological lipid  
776 bilayers: insights from all-atom molecular dynamics simulations. *J. Mol. Model.* 25, 1–13.  
777 <https://doi.org/10.1007/s00894-019-3964-0>
- 778 Subczynski, W.K., Pasenkiewicz-Gierula, M., Widomska, J., Mainali, L., Raguz, M., 2017. High  
779 cholesterol/low cholesterol: Effects in biological membranes Review. *Cell Biochem. Biophys.* 75, 369.  
780 <https://doi.org/10.1007/S12013-017-0792-7>
- 781 Tang, P., Xu, Y., 2002. Large-scale molecular dynamics simulations of general anesthetic effects on the ion  
782 channel in the fully hydrated membrane: The implication of molecular mechanisms of general  
783 anesthesia. *Proc. Natl. Acad. Sci.* 99, 16035–16040. <https://doi.org/10.1073/PNAS.252522299>
- 784 Taylor, D.M., Eger, E.I., Bickler, P.E., 1999. Halothane, But Not the Nonimmobilizers Perfluoropentane and  
785 1,2-Dichlorohexafluorocyclobutane, Depresses Synaptic Transmission in Hippocampal CA1 Neurons  
786 in Rats. *Anesth. Analg.* 89, 1040. <https://doi.org/10.1213/00000539-199910000-00041>

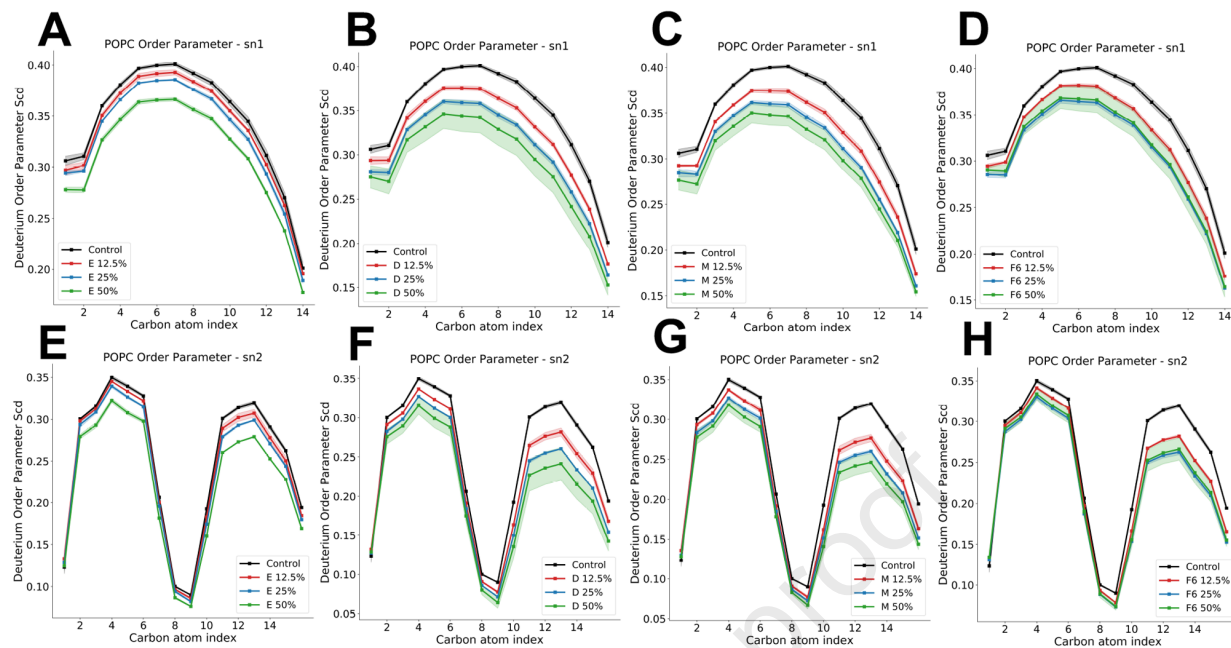
- 787 TJ, M., 1978. The effect of cholesterol on the structure of phosphatidylcholine bilayers. *Biochim. Biophys.*  
788 *Acta* 513, 43–58. [https://doi.org/10.1016/0005-2736\(78\)90110-4](https://doi.org/10.1016/0005-2736(78)90110-4)
- 789 Tsuchiya, H., Mizogami, M., 2013. Interaction of local anesthetics with biomembranes consisting of  
790 phospholipids and cholesterol: Mechanistic and clinical implications for anesthetic and cardiotoxic  
791 effects. *Anesthesiol. Res. Pract.* <https://doi.org/10.1155/2013/297141>
- 792 Tu, K., Tarek, M., Klein, M.L., Scharf, D., 1998. Effects of Anesthetics on the Structure of a Phospholipid  
793 Bilayer: Molecular Dynamics Investigation of Halothane in the Hydrated Liquid Crystal Phase of  
794 Dipalmitoylphosphatidylcholine. *Biophys. J.* 75, 2123–2134. [https://doi.org/10.1016/S0006-3495\(98\)77655-6](https://doi.org/10.1016/S0006-3495(98)77655-6)
- 796 Van Rossum, G., Drake, F.L., 2009. *Python 3 Reference Manual*.
- 797 Vauquelin, G., Packeu, A., 2009. Ligands, their receptors and ... plasma membranes. *Mol. Cell. Endocrinol.*  
798 311, 1–10. <https://doi.org/10.1016/j.mce.2009.07.022>
- 799 Watson, M.C., Penev, E.S., Welch, P.M., Brown, F.L.H., 2011. Thermal fluctuations in shape, thickness, and  
800 molecular orientation in lipid bilayers. *J. Chem. Phys.* 135, 244701. <https://doi.org/10.1063/1.3660673>
- 801 Wu, E.L., Cheng, X., Jo, S., Rui, H., Song, K.C., Dávila-Contreras, E.M., Qi, Y., Lee, J., Monje-Galvan, V.,  
802 Venable, R.M., Klauda, J.B., Im, W., 2014. CHARMM-GUI Membrane Builder toward realistic  
803 biological membrane simulations. *J. Comput. Chem.* 35, 1997–2004. <https://doi.org/10.1002/jcc.23702>
- 804 Yamakura, T., Bertaccini, E., Trudell, J.R., Harris, R.A., 2003. Anesthetics and Ion Channels: Molecular  
805 Models and Sites of Action1. <http://dx.doi.org/10.1146/annurev.pharmtox.41.1.23> 41, 23–51.  
806 <https://doi.org/10.1146/ANNUREV.PHARMTOX.41.1.23>
- 807 Yamamoto, E., Akimoto, T., Shimizu, H., Hirano, Y., Yasui, M., Yasuoka, K., 2012. Diffusive nature of  
808 xenon anesthetic changes properties of a lipid bilayer: Molecular dynamics simulations. *J. Phys. Chem.*  
809 *B* 116, 8989–8995. <https://doi.org/10.1021/jp303330c>
- 810 Zachowski, A., 1993. Phospholipids in animal eukaryotic membranes: Transverse asymmetry and  
811 movement. *Biochem. J.* 294, 1–14. <https://doi.org/10.1042/bj2940001>
- 812 Zhuang, X., Makover, J.R., Im, W., Klauda, J.B., 2014. A systematic molecular dynamics simulation study  
813 of temperature dependent bilayer structural properties. *Biochim. Biophys. Acta - Biomembr.* 1838,  
814 2520–2529. <https://doi.org/10.1016/j.bbamem.2014.06.010>

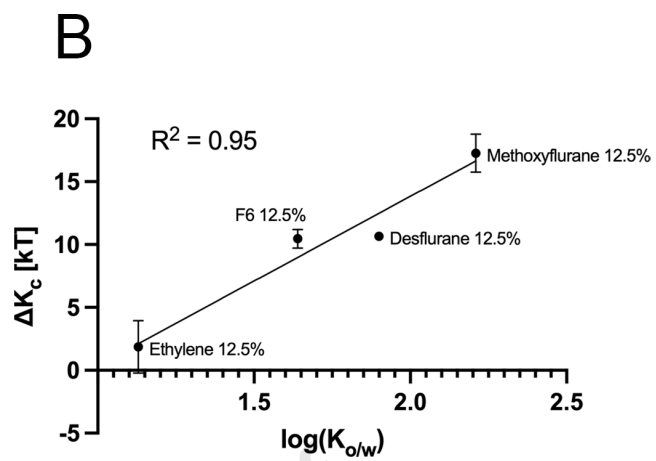
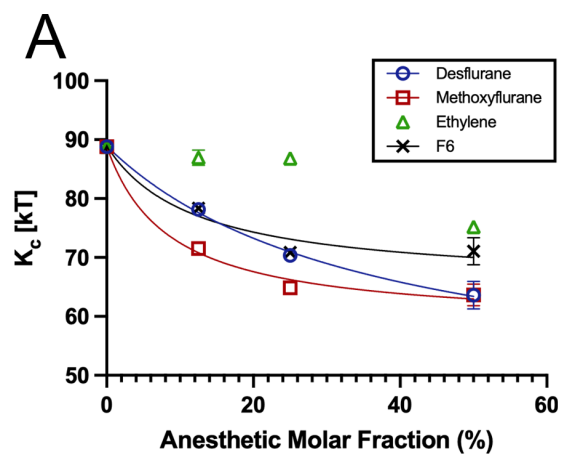












## Highlights

- Molecular simulations of lipid bilayer interaction with volatile anesthetics
- Comparison of volatile anesthetics' and nonimmobilizers' effects on lipid bilayers
- Ligand-dependent partitioning of the compounds in the lipid phase
- Effects on bilayer thickness, stiffness and lipid order upon ligand partitioning

Journal Pre-proof

**Key resources table**

REAGENT or RESOURCE	SOURCE	IDENTIFIER
Software and algorithms		
GROMACS version 2020.4	(Abraham et al., 2015)	<a href="https://manual.gromacs.org/">https://manual.gromacs.org/</a>
CHARMM-GUI Membrane Builder	(Jo et al., 2009)	<a href="https://charmm-gui.org/?doc=input">https://charmm-gui.org/?doc=input</a>
MDAnalysis version 2.0.0	Michaud-Agrawal et al., 2011)	<a href="https://www.mdanalysis.org">https://www.mdanalysis.org</a>
Python version 3.7	(Van Rossum and Drake, 2009)	<a href="https://www.python.org/downloads/release/python-370/">https://www.python.org/downloads/release/python-370/</a>
OpenStructure version 2.3	(Biasini et al., 2013)	<a href="https://openstructure.org">https://openstructure.org</a>
VMD Version 1.9.3	(Humphrey et al., 1996)	<a href="https://www.ks.uiuc.edu/Research/vmd/">https://www.ks.uiuc.edu/Research/vmd/</a>
Methodology for determining elastic properties of lipid assemblies from MD simulations	(Johner et al., 2016)	<a href="http://dx.doi.org/10.1186/s12859-016-1003-z">http://dx.doi.org/10.1186/s12859-016-1003-z</a>